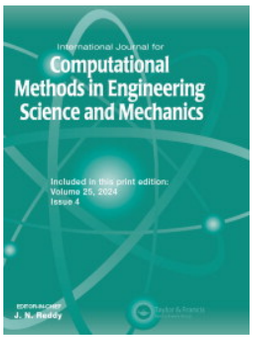

International Journal for Computational Methods in Engineering Science and Mechanics

ISSN: (Print) (Online) Journal homepage: www.tandfonline.com/journals/ucme20

Stability and dynamic analyses of hybrid laminates using refined higher-order zigzag theory

Dhiraj Biswas, Rudraprasad Bhattacharyya & Chaitali Ray

To cite this article: Dhiraj Biswas, Rudraprasad Bhattacharyya & Chaitali Ray (04 Jul 2024): Stability and dynamic analyses of hybrid laminates using refined higher-order zigzag theory, International Journal for Computational Methods in Engineering Science and Mechanics, DOI: 10.1080/15502287.2024.2372821

To link to this article: https://doi.org/10.1080/15502287.2024.2372821

INTERNATIONAL JOURNAL FOR COMPUTATIONAL METHODS IN ENGINEERING SCIENCE AND MECHANICS
https://doi.org/10.1080/15502287.2024.2372821

Stability and dynamic analyses of hybrid laminates using refined higher-order zigzag theory

Dhiraj Biswas[a], Rudraprasad Bhattacharyya[b], and Chaitali Ray[c]

[a]University of Salford, Salford, UK; [b]Cronus Technology Inc, Houston, Texas, USA; [c]Indian Institute of Engineering Science and Technology Shibpur, Shibpur, India

ABSTRACT

This article presents a comparative study on the stability and dynamic response of hybrid laminated composite plates over monolithically produced laminated composite plates. A Refined Higher-order Zigzag Theory (RHZT) is formulated and implemented using finite element method for the analysis of hybrid laminates. This formulation considers both the interlaminar shear stress continuity and shear-free boundary conditions at surfaces of the plates. The numerical implementation employs C^0 continuous eight-noded isoparametric plate elements considering geometric nonlinearity. The element stiffness matrix is formulated to consider both the linear and nonlinear terms of the strain-displacement equations. Derivation of the consistent mass matrix for a plate element is presented following the approximation of total kinetic energy and utilising Hamilton's principle. Numerical examples are provided to demonstrate buckling and free vibration analyses (as eigenvalue problems). The results are numerically verified and validated using data from published literature. Finally, parametric studies are presented to demonstrate the effectiveness of fibre hybridisation approach on the buckling and free vibration behaviour of laminated composites.

KEYWORDS

Hybrid laminated plate; refined higher-order zigzag theory; finite element method; buckling analysis; free vibration analysis

1. Introduction

In the cost-effective smart design of laminated fibre composite structures, hybridisation of fibre appears to be one of the promising approaches. In this approach incorporating layups with different materials and fibre orientations enables enhancement of tailor-made properties that cannot be achieved by single filamentary of material. These properties may include superior strength to weight ratio, durability, corrosion resistance and adaptability. However, the laminated composites are weak in shear as compared to the extensional rigidity. This inevitable limitation along with multiple filamentary combination within hybrid laminates increases the complexities to analyse this kind of structure accurately. As a consequence, the effect of shear deformations of laminated structures requires a complex numerical model to evaluate the realistic responses. Typically implementation of shear deformation formulation within the computational framework makes the analyses more challenging as that brings in additional degrees-of-freedom. Moreover, in engineering applications, such as automotive and marine and civil infrastructure sectors, laminated composite structures are not only subjected to static loads, but also to dynamic loads. Therefore, for the purpose of safe structural design, both stability and dynamic analyses need to be performed before practical application of hybrid laminated composites. In the stability analysis the buckling response of the composite structure is evaluated. On the other hand, free vibration analysis is performed to calculate the natural frequencies of the structure.

The Classical Laminate Theory (CLT) of Love-Kirchhoff [1] was significantly improved upon by several researchers in the second half of the last century. The problem of buckling and vibration response of laminates were evaluated using three-dimensional elasticity theory [2, 3]. However, two-dimensional theories gained significant popularity due to the prohibitive computational cost of three-dimensional theories [4]. After the introduction of the First-order Shear Deformation Theory (FSDT) [5, 6] composite laminates were analysed using two-dimensional methods (for example, plate theory), under different geometric and material effects [7–9], strain states [10] and boundary conditions [11, 12].

CONTACT Dhiraj Biswas d.biswas@salford.ac.uk University of Salford, Salford, UK.

However, due to dependence on the magnitude of the shear correction factor FSDT is unable to accurately predict laminate response. To overcome this limitation, Higher-order Shear Deformation Theory (HSDT) [13–15] was introduced by considering the higher order terms of Taylor's series expansion of the displacement fields within the laminate. After implementing the HSDT in Finite Element Method (FEM), researchers performed buckling and free vibration analysis of composite laminates with different geometric conditions and consideration of material heterogeneity and nonlinearity [16–22]. Over the past couple of decades the HSDT has been further refined to increase numerical accuracy [23–26]. The HSDT was developed based on the assumptions that lead to discontinuity of transverse shear stress in the laminate towards the through-thickness direction. This through-thickness transverse shear stress discontinuity has an insignificant impact on the numerical solution of thin laminates. But this stress discontinuity leads to erroneous results for thick plates and hybrid laminates as the interlaminar stress equilibrium condition is not satisfied.

To alleviate the issue of discontinuity in the transverse shear stress researchers proposed several methods such as layer-wise plate models [27–30], Discrete Layer Theory (DLT) [27–31]. These approaches are computationally expensive to employ for thicker laminates due to increase in the number of unknown variables. The complexity in numerical analysis was reduced by the introduction of various zigzag (ZZ) models, developed by Di Sciuva [32, 33], Liu and Li [34], Murakami [35], Tessler *et al.* [36–39].

In most of the zigzag models the in-plane displacement field is represented with a combination of global and local displacement function. The major benefit of this type of model is that it satisfies the transverse shear stress continuity conditions at the layer interfaces. In addition, the number of unknowns in these plate models remain independent of the number of layers. The fundamental features of all the Refined ZZ plate theories are similar, but varies only in the mathematical expression of the refinement. Earlier development of the zigzag formulations primarily considered FSDT as the global displacement field. The FE implementation of the higher-order zigzag theories require C^1 continuity of transverse displacements at the nodes. However, in practice, C^0 continuity is encouraged [40]. Thus, it is necessary to develop a FE model as a combination of HSDT and a layer-wise (LW) linear zigzag displacement field using isoparametric plate bending element for the analysis of composite laminates efficiently. In the present state of knowledge several variants of ZZ models have been employed in the prediction of buckling loads [41–45] and natural frequency [46–51] for laminated composite structures. These studies focused only on a single type of composite material. To the best of authors' knowledge, investigation on buckling and free vibration analysis of hybrid laminates due to the effect of fibre hybridisation has remained unexplored. This article employs a Refined Higher-order Zigzag Theory (RHZT) by considering the warping effect [52] which is numerically implemented considering C^0 continuity at the layer interfaces of hybrid laminates. The hybrid laminate analysed in this study comprises carbon and glass fibres with epoxy resin base. Being stronger and stiffer, the carbon fabrics are chosen to be placed at the outermost laminate surfaces, whereas glass fabrics in the inner layups of the laminate. In this article, the framework is further extended to calculate geometric stiffness and mass matrices of the plate bending element by incorporating nonlinear strain components. The hybrid laminate is modelled with the eight-noded isoparametric quadratic element during finite element (FE) formulation. Two examples of parametric studies are carried out by considering the variations in number of layers, layer thickness, layup sequence, aspect ratio and percentage of hybridisation of the hybrid laminates. The numerical solutions obtained using the proposed framework are compared with data available in published literature. Finally, the efficiency of the fibre hybridisation approach is evaluated for laminated composite plates.

This article is organised as follows. A brief outline of the refined higher-order theory is discussed in Section 2. Numerical implementation of the proposed formulation is discussed in Section 3. The description of numerical verification using two types of cross-ply laminates is provided in Section 4. Parametric studies on the effectiveness of hybrid laminates are discussed in Section 5. Section 6 provides concluding remarks and directions for future research.

2. Mathematical formulation

Let a hybrid laminate of width a, length b, and thickness h be presented in a Cartesian coordinate system $\mathbf{X}$ as shown in Figure 1. The in-plane displacement fields ($\mathbf{u}$) of the laminate due to loading can be obtained analytically by considering the global and local contributions of the displacement fields as Eq. (1).

$$\mathbf{u}^{(kl)}(\mathbf{X}) = \mathbf{u}_g^{(l)}(\mathbf{X}) + \bar{\mathbf{u}}_l^{(k)}(\mathbf{X}) \tag{1}$$

where, the global contribution is expressed as a cubic polynomial function through the thickness of laminate and denoted as $\mathbf{u}_g^{(l)}$. On the other hand, the local

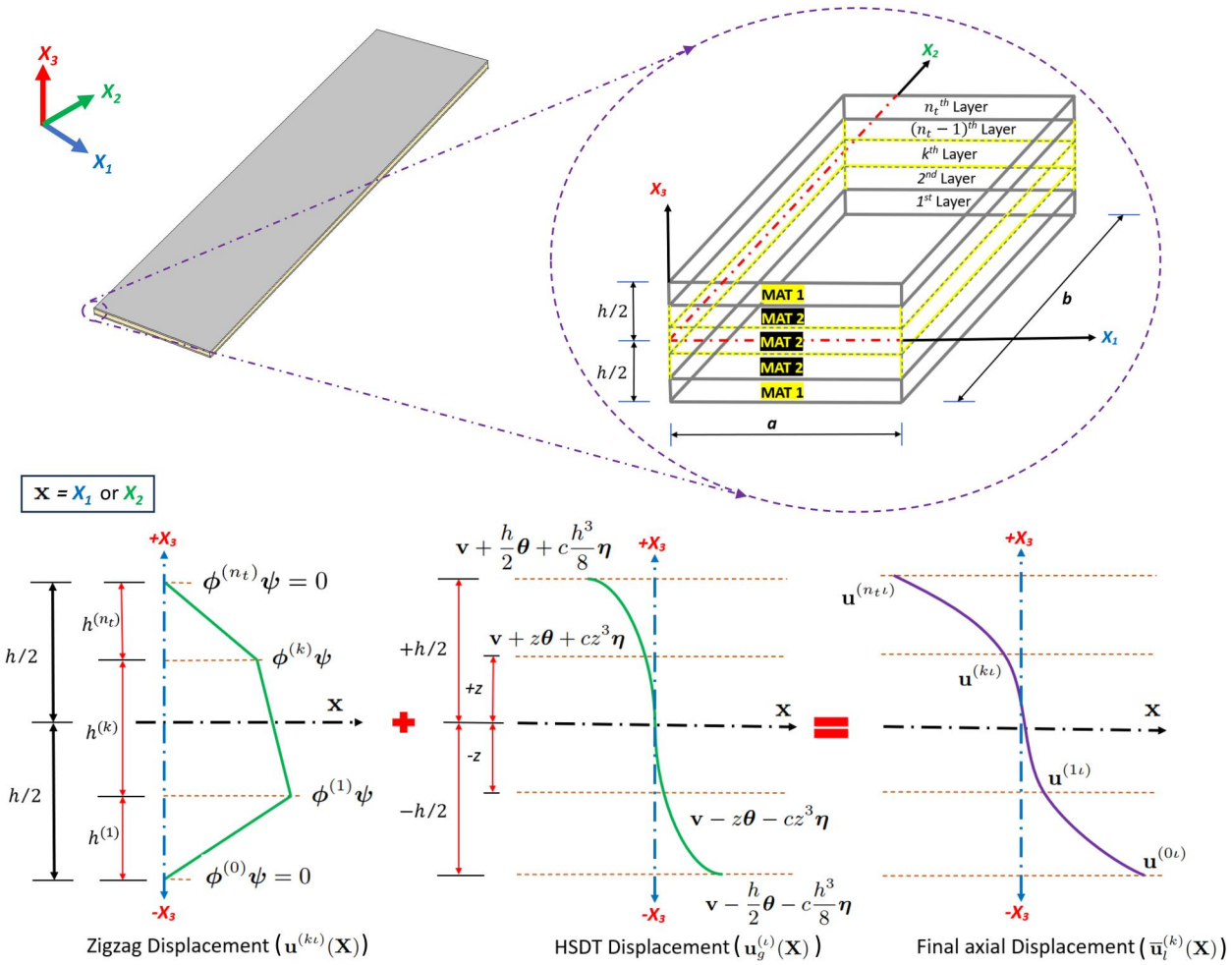

Figure 1. Schematic diagram of a hybrid FRP laminate.

contribution of the displacement fields is captured by the ZZ function (denoted by $\bar{\mathbf{u}}_l^{(k)}$). The superscript k denotes the sequence of layups in the laminate. The cubic polynomial function for global displacement field calculation is based on the third-order shear deformation theory (HSDT), which is obtained by the Taylor series expansion as Eq. (2).

$$\begin{aligned}\mathbf{u}_g^{(\iota)}(\mathbf{X}) &= \mathbf{u}^{(0)}(\mathbf{X}) + (z\mathbf{u}^{(1)}(\mathbf{x}) + z^2\mathbf{u}^{(2)}(\mathbf{x}) + z^3\mathbf{u}^{(3)}(\mathbf{x})) \\ &= \mathbf{v}(\mathbf{X}) + z^\iota\mathbf{u}^{(\iota)}(\mathbf{x})\end{aligned} \tag{2}$$

Here, $\mathbf{v}(\mathbf{X})$ is used to substitute the term $\mathbf{u}^{(0)}(\mathbf{X})$ and the remaining part is written in a generalised notation. The field variables that vary along all three axes directions are denoted by $\mathbf{X}$, whereas the variables which vary only in the directions x_1 and x_2 are denoted by $\mathbf{x}$. The local displacement fields are calculated according to the RHZT and can be written as Eq. (3).

$$\bar{\mathbf{u}}_l^{(k)}(\mathbf{X}) = \phi^{(k)}(x_3)\boldsymbol{\psi}(\mathbf{x}) \tag{3}$$

Consider, z_k is the vertical coordinate of the k-th interface ($k = 1 \cdots n_t$), where $z_k \leq z \leq z_{k+1}$ and n_t is the total number of layups. Considering the displacement field within the elastic limit of the material, the transverse shear stresses should vanish at the top and bottom surfaces of the laminate. Hence, the corresponding transverse shear strain components need to be zero at the boundary surfaces. Similarly, the zigzag function assumes zero values at top and bottom surfaces of the laminate. Satisfying the condition of no transverse shear stress and zigzag effect at the free surfaces of the laminate, the Eq. (1) can be written as Eq. (4).

$$\mathbf{u}^{(k\iota)}(\mathbf{X}) = \mathbf{v}(\mathbf{X}) + z\boldsymbol{\theta}(\mathbf{x}) + cz^3\boldsymbol{\eta}(\mathbf{x}) + \phi^{(k)}(x_3)\boldsymbol{\psi}(\mathbf{x}) \tag{4}$$

where, $\mathbf{v}(\mathbf{X})$ are the displacement components along the axes x_1, x_2 and x_3 and can explicitly be written as v_1,v_2 and v_3. In Eq. (4), $c = -\frac{4}{3h^2}$. The rotational components about coordinate axes x_1 and x_2 are denoted by the variable $\boldsymbol{\theta}$. The warping function ($\boldsymbol{\eta}$) is used in the higher-order theory to maintain the desired C^0 continuity. The components $\phi^{(k)}$ denote a layerwise

linear ZZ function and $\boldsymbol{\psi}$ is a primary kinematic variable defining the amplitude of the ZZ function on the plate. The last term of Eq. (4) defines the zigzag displacements (as shown in Figure 1) which includes the corrections to the in-plane displacement fields associated with heterogeneity of laminate across the thickness direction. The linear strain vectors associated with the governing displacement fields (written in the Eq. (4)) are given by,

$$\begin{aligned}\boldsymbol{\epsilon}^{(k)}(\mathbf{X}) &= \nabla \mathbf{u}^{(k\imath)}(\mathbf{X}) \\ &= \nabla \mathbf{v}(\mathbf{X}) + z\nabla\boldsymbol{\theta}(\mathbf{x}) + cz^3\nabla\boldsymbol{\eta}(\mathbf{x}) \\ &\quad + \nabla\phi^{(k)}(x_3)\nabla\boldsymbol{\psi}(\mathbf{x}) \end{aligned} \tag{5}$$

Now, the in-plane ($\boldsymbol{\epsilon}_p$) and transverse shear ($\boldsymbol{\epsilon}_t$) strain components can be defined as,

$$\begin{aligned}\boldsymbol{\epsilon}^{(k)}(\mathbf{X}) = \begin{Bmatrix} \boldsymbol{\epsilon}_p \\ \boldsymbol{\epsilon}_t \end{Bmatrix}^{(k)} &= \begin{Bmatrix} \boldsymbol{\epsilon}_m \\ \mathbf{0} \end{Bmatrix} + \begin{Bmatrix} \boldsymbol{\epsilon}_b \\ \boldsymbol{\epsilon}_s \end{Bmatrix} + \begin{Bmatrix} \boldsymbol{\epsilon}_w \\ \boldsymbol{\epsilon}_{sw} \end{Bmatrix} \\ &\quad + \begin{Bmatrix} \boldsymbol{\epsilon}_{mb\phi} \\ \boldsymbol{\epsilon}_{s\phi} \end{Bmatrix}^{(k)} = \begin{bmatrix} S_p^{(k)} & 0 \\ 0 & S_t^{(k)} \end{bmatrix} \begin{Bmatrix} \hat{\boldsymbol{\epsilon}}_p \\ \hat{\boldsymbol{\epsilon}}_t \end{Bmatrix}^{(k)} \end{aligned} \tag{6}$$

where, the strain vectors associated to the membrane, bending and warping effects are represented by $\boldsymbol{\epsilon}_m$, $\boldsymbol{\epsilon}_b$ and $\boldsymbol{\epsilon}_w$, respectively. The transverse shear strain vectors are defined by $\boldsymbol{\epsilon}_s$ and $\boldsymbol{\epsilon}_{sw}$. The longitudinal and transverse shear strain vectors derived from the zigzag effect are represented by $\boldsymbol{\epsilon}_{mb\phi}$ and $\boldsymbol{\epsilon}_{s\phi}$, respectively. The generalised in-plane and transverse shear strain vectors at each layer are represented as,

$$\{\hat{\boldsymbol{\epsilon}}_p\}^{(k)} = \left\{ \hat{\boldsymbol{\epsilon}}_m \quad \hat{\boldsymbol{\epsilon}}_b \quad \hat{\boldsymbol{\epsilon}}_w \quad \hat{\boldsymbol{\epsilon}}_{mb\phi}^{(k)} \right\}^\top \tag{7}$$

$$\{\hat{\boldsymbol{\epsilon}}_t\}^{(k)} = \left\{ \hat{\boldsymbol{\epsilon}}_s \quad \hat{\boldsymbol{\epsilon}}_{sw} \quad \hat{\boldsymbol{\epsilon}}_{s\phi}^{(k)} \right\}^\top \tag{8}$$

Similarly, the corresponding coefficient terms represented as blocks and are defined as,

$$S_p^{(k)} = \begin{bmatrix} S_m & S_b & S_w & S_{mb\phi}^{(k)} \end{bmatrix} \tag{9}$$

and

$$S_t^{(k)} = \begin{bmatrix} S_s & S_{sw} & S_{s\phi}^{(k)} \end{bmatrix} \tag{10}$$

where, $S_m = \begin{bmatrix} 1 & 0 & 0 \\ 0 & 1 & 0 \\ 0 & 0 & 1 \end{bmatrix}$, $S_b = \begin{bmatrix} z & 0 & 0 \\ 0 & z & 0 \\ 0 & 0 & z \end{bmatrix}$, $S_w = \begin{bmatrix} z^3 & 0 & 0 \\ 0 & z^3 & 0 \\ 0 & 0 & z^3 \end{bmatrix}$, $S_{mb\phi}^{(k)} = \begin{bmatrix} \phi_1^{(k)} & 0 & 0 & 0 \\ 0 & \phi_2^{(k)} & 0 & 0 \\ 0 & 0 & \phi_1^{(k)} & \phi_2^{(k)} \end{bmatrix}$, $S_s = \begin{bmatrix} 1 & 0 \\ 0 & 1 \end{bmatrix}$, $S_{sw} = \begin{bmatrix} z^2 & 0 \\ 0 & z^2 \end{bmatrix}$, and, $S_{s\phi}^{(k)} = \begin{bmatrix} \beta_1^{(k)} & 0 \\ 0 & \beta_2^{(k)} \end{bmatrix}$.

Now the constitutive relation for the stress tensors can be expressed as,

$$\boldsymbol{\sigma}^{(k)} = \begin{Bmatrix} \hat{\boldsymbol{\sigma}}_p \\ \hat{\boldsymbol{\sigma}}_t \end{Bmatrix}^{(k)} = \begin{bmatrix} \mathbf{D}_p & \mathbf{0} \\ \mathbf{0} & \mathbf{D}_t \end{bmatrix} \begin{Bmatrix} \hat{\boldsymbol{\epsilon}}_p \\ \hat{\boldsymbol{\epsilon}}_t \end{Bmatrix}^{(k)} = \mathbf{D}\boldsymbol{\epsilon}^{(k)} \tag{11}$$

where, $\hat{\boldsymbol{\sigma}}_p$ and $\hat{\boldsymbol{\sigma}}_t$ are in-plane and transverse shear stress tensors, respectively. The generalised constitutive tensor related to the in-plane and transverse shear stress and strain, $\mathbf{D}_p$ and $\mathbf{D}_t$, are given by Eqs. (12) and (13).

$$\mathbf{D}_p = \begin{bmatrix} \int_z (S_m)^\top D_p^{(k)} S_m dz & \int_z (S_{mb\phi}^{(k)})^\top D_p^{(k)} S_{mb\phi}^{(k)} dz & \int_z (S_m)^\top D_p^{(k)} S_w dz & \int_z (S_m)^\top D_p^{(k)} S_{mb\phi}^{(k)} dz \\ \int_z (S_b)^\top D_p^{(k)} S_m dz & \int_z (S_b)^\top D_p^{(k)} S_b dz & \int_z (S_b)^\top D_p^{(k)} S_w dz & \int_z (S_b)^\top D_p^{(k)} S_{mb\phi}^{(k)} dz \\ \int_z (S_w)^\top D_p^{(k)} S_m dz & \int_z (S_w)^\top D_p^{(k)} S_b dz & \int_z (S_w)^\top D_p^{(k)} S_w dz & \int_z (S_w)^\top D_p^{(k)} S_{mb\phi}^{(k)} dz \\ \int_z (S_{mb\phi}^{(k)})^\top D_p^{(k)} S_m dz & \int_z (S^{(k)}{}_{mb\phi})^\top D_p^{(k)} S_b dz & \int_z (S_{mb\phi}^{(k)})^\top D_p^{(k)} S_w dz & \int_z (S_{mb\phi}^{(k)})^\top D_p^{(k)} S_{mb\phi}^{(k)} dz \end{bmatrix} \tag{12}$$

and

$$\mathbf{D}_t = \begin{bmatrix} \int_z (S_s)^\top D_t^{(k)} S_s dz & \int_z (S_s)^\top D_t^{(k)} S_{sw} dz & \int_z (S_s)^\top D_t^{(k)} S_{s\phi} dz \\ \int_z (S_{sw})^\top D_t^{(k)} S_s dz & \int_z (S_{sw})^\top D_t^{(k)} S_{sw} dz & \int_z (S_{sw})^\top D_t^{(k)} S_{s\phi} dz \\ \int_z (S_{s\phi})^\top D_t^{(k)} S_s dz & \int_z (S_{s\phi})^\top D_t^{(k)} S_{sw} dz & \int_z (S_{s\phi})^\top D_t^{(k)} S_{s\phi} dz \end{bmatrix} \tag{13}$$

The ZZ function (Ref. [52]) along the thickness of the laminate employed in this study for each layup is defined as,

$$\phi^{(k)}(x_3) = \frac{1}{2}(1-\xi^{(k)})\bar{\phi}^{(k-1)} + \frac{1}{2}(1+\xi^{(k)})\bar{\phi}^{(k)} = \frac{\bar{\phi}^{(k)}+\phi^{(k-1)}}{2} + \frac{\bar{\phi}^{(k)}-\phi^{(k-1)}}{2}\xi^{(k)} \tag{14}$$

where, $\bar{\phi}^{(k)}$ and $\bar{\phi}^{(k-1)}$ are the ZZ function values at k-th and $(k-1)$-th interfaces, respectively. It is assumed that the ZZ function vanishes at the free surfaces, such as $\bar{\phi}^{(0)} = \bar{\phi}^{(n_t)} = 0$. Here, $\xi^{(k)}$ is calculated as $\xi^{(k)} = \frac{2(z-z^{(k-1)})}{h^{(k)}} - 1$. The slope of the ZZ function, $\boldsymbol{\beta}^{(k)}$, is constant at each layer and defined as,

$$\boldsymbol{\beta}^{(k)}(x_3) = \nabla\phi^{(k)}(x_3) = \frac{\bar{\phi}^{(k)}-\bar{\phi}^{(k-1)}}{h^{(k)}} \tag{15}$$

3 Numerical implementation

The plate element has been formulated using an eight-noded isoparametric quadratic plate bending element considering nine degrees-of-freedom per node. The nodal deformations are expressed in terms of the nodal displacements and rotations as Eq. (16).

$$\{\delta\} = \{v_1\ v_2\ v_3\ \theta_1\ \theta_2\ \eta_1\ \eta_2\ \psi_1\ \psi_2\}^\top = \sum_{i=1}^{8}\mathcal{N}_i\delta_i \tag{16}$$

In Eq. (16), $\mathcal{N}_i$ is the shape function at the associated node of the element and δ_i is the nodal deformation. The element stiffness matrix ($\mathbf{K}_e$) for the plate element is obtained as,

$$\mathbf{K}_e = \int_A \mathbf{B}^\top\mathbf{D}\mathbf{B}\ dA \tag{17}$$

where, $\mathbf{B}$ and A are the generalised strain-displacement matrix and the area of the element, respectively.

3.1. Stability analysis

The stability analysis is performed as an eigen-value problem. In this case the geometric stiffness matrix needs to be computed. For this purpose, the exact strain-displacement relations involving nonlinear terms are considered to derive the governing equilibrium equation. In order to study the stability problem of laminated plates, the second order potential energy of initially stressed plates has to be determined. The initial stress works for the nonlinear gradient of displacements and can be expressed as,

$$\mathcal{V}_E^{(2)} = \int_V (\boldsymbol{\sigma}^0)^\top : \boldsymbol{\epsilon}_{\mathrm{NL}}\ dV \tag{18}$$

where, $\mathcal{V}_E^{(2)}$ is the second order potential energy, $\boldsymbol{\sigma}^0 = [\sigma_{11}^0\ \ \sigma_{22}^0\ \ \tau_{12}^0]^\top$ and $\boldsymbol{\epsilon}_{\mathrm{NL}}$ represents the nonlinear strains. The nonlinear strains used in this paper are derived by using the Von Kármán nonlinear strains which can be expressed as,

$$\boldsymbol{\epsilon}_{\mathrm{NL}} = \frac{1}{2}(\nabla\mathbf{u})(\nabla\mathbf{u})^\top \tag{19}$$

Finally, the potential of second order displacement is calculated by substituting Eq. (19) into Eq. (18) and can be expressed as:

$$\mathcal{V}_E^{(2)} = \frac{1}{2}\int_V (\boldsymbol{\sigma}^0)^\top : (\nabla\mathbf{u})(\nabla\mathbf{u})^\top\ dV \tag{20}$$

By substituting the individual terms in Eq. (20) and rearranging them, the second order potential energy can be written as,

$$\mathcal{V}_E^{(2)} = \frac{1}{2}\int_V \Big[(\nabla\mathbf{v})^\top\hat{\boldsymbol{\sigma}}^0\nabla\mathbf{v} + z^2\nabla\boldsymbol{\theta}^\top\hat{\boldsymbol{\sigma}}^0\nabla\boldsymbol{\theta} + c^2z^6\nabla\boldsymbol{\eta}^\top\hat{\boldsymbol{\sigma}}^0\nabla\boldsymbol{\eta} + (\phi^{(k)})^2\nabla\boldsymbol{\psi}^\top\hat{\boldsymbol{\sigma}}^0\nabla\boldsymbol{\psi}\Big]dV \tag{21}$$

Finally, the second order potential energy is obtained as

$$\mathcal{V}_E^{(2)} = \frac{1}{2}\int_A \left[z(\nabla\mathbf{v})^\top\hat{\boldsymbol{\sigma}}^0\nabla\mathbf{v} + \frac{z^3}{3}\nabla\boldsymbol{\theta}^\top\hat{\boldsymbol{\sigma}}^0\nabla\boldsymbol{\theta} + c^2\frac{z^7}{7}\nabla\boldsymbol{\eta}^\top\hat{\boldsymbol{\sigma}}^0\nabla\boldsymbol{\eta} + \left[\int(\phi^{(k)})^2dz\right]\nabla\boldsymbol{\psi}^\top\hat{\boldsymbol{\sigma}}^0\nabla\boldsymbol{\psi}\right]dA \tag{22}$$

Here, dA represents the area of the laminate and $\hat{\boldsymbol{\sigma}}^0 = \begin{bmatrix}\sigma_{11}^0 & \tau_{12}^0\\ \tau_{12}^0 & \sigma_{22}^0\end{bmatrix}$. By collecting all the terms of the Eq. (22) in matrix form, it can be expressed as,

$$\mathcal{V}_E^{(2)} = \frac{1}{2}\int_{\boldsymbol{A}} [\,(\nabla\nu_1)^\top \quad (\nabla\nu_2)^\top \quad (\nabla\nu_3)^\top \quad (\nabla\theta_1)^\top \quad (\nabla\theta_2)^\top \quad (\nabla\eta_1)^\top \quad (\nabla\eta_2)^\top \quad (\nabla\psi_1)^\top \quad (\nabla\psi_2)^\top\,]\mathbf{S}^0 \begin{bmatrix} \nabla\nu_1 \\ \nabla\nu_2 \\ \nabla\nu_3 \\ \nabla\theta_1 \\ \nabla\theta_2 \\ \nabla\eta_1 \\ \nabla\eta_2 \\ \nabla\psi_1 \\ \nabla\psi_2 \end{bmatrix} dA \tag{23}$$

where, $\mathbf{S}^0$ is a banded matrix of size 18×18 as

$$\mathbf{S}^0 = \begin{bmatrix} z\hat{\boldsymbol{\sigma}}^0 & \mathbf{0} & \mathbf{0} & \mathbf{0} & \mathbf{0} & \mathbf{0} & \mathbf{0} & \mathbf{0} & \mathbf{0} \\ & z\hat{\boldsymbol{\sigma}}^0 & \mathbf{0} & \mathbf{0} & \mathbf{0} & \mathbf{0} & \mathbf{0} & \mathbf{0} & \mathbf{0} \\ & & z\hat{\boldsymbol{\sigma}}^0 & \mathbf{0} & \mathbf{0} & \mathbf{0} & \mathbf{0} & \mathbf{0} & \mathbf{0} \\ & & & \frac{z^3}{3}\hat{\boldsymbol{\sigma}}^0 & \mathbf{0} & \mathbf{0} & \mathbf{0} & \mathbf{0} & \mathbf{0} \\ \text{Symm.} & & & & \frac{z_k^3}{3}\hat{\boldsymbol{\sigma}}^0 & \mathbf{0} & \mathbf{0} & \mathbf{0} & \mathbf{0} \\ & & & & & \frac{z_k^7}{7}\hat{\boldsymbol{\sigma}}^0 & \mathbf{0} & \mathbf{0} & \mathbf{0} \\ & & & & & & \frac{z_k^7}{7}\hat{\boldsymbol{\sigma}}^0 & \mathbf{0} & \mathbf{0} \\ & & & & & & & \left[\int_{z_{k-1}}^{z_k} (\phi_1^{(k)})^2 dz\right]\hat{\boldsymbol{\sigma}}^0 & \mathbf{0} \\ & & & & & & & & \left[\int_{z_{k-1}}^{z_k} (\phi_2^{(k)})^2 dz\right]\hat{\boldsymbol{\sigma}}^0 \end{bmatrix} \tag{24}$$

where, $\boldsymbol{0}$ is a null matrix of size 2×2. Since the scope is to introduce the finite element approximation, it is convenient to convert the vector of symmetric gradients as $\nabla\mathbf{u} = \nabla^s\boldsymbol{\delta}$. Finally, the second order potential energy (Eq. (23)) can be expressed in matrix form by implementing the finite element approximation as,

$$\begin{aligned}\mathcal{V}_E^{(2)} &= \frac{1}{2}\int_A (\nabla\mathbf{u}^{(k)})^\top \mathbf{S}^0 (\nabla\mathbf{u}^{(k)}) dA \\ &= \frac{1}{2}\nabla\boldsymbol{\delta}^\top \left[\int_A (\nabla\mathcal{N})^\top \mathbf{S}^0 (\nabla\mathcal{N}) dA\right]\nabla\boldsymbol{\delta} = \frac{1}{2}\left[\int_A \mathbf{G}^\top \mathbf{S}^0 \mathbf{G} dA\right]\nabla\boldsymbol{\delta}\end{aligned} \tag{25}$$

Thus, the geometric stiffness matrix $\mathbf{K}_g^e$ is defined by,

$$\mathbf{K}_g^e = \int_A \mathbf{G}^\top \mathbf{S}^0 \mathbf{G}\ dA \tag{26}$$

Combining geometric stiffness matrix and elastic stiffness matrix, the dynamic equilibrium equation leads to the governing equations for dynamic analysis.

$$([\mathbf{K}] - \lambda[\mathbf{K}_G])\{\boldsymbol{\delta}\} = \mathbf{0} \tag{27}$$

in which, $[\mathbf{K}]$ and $[\mathbf{K}_G]$ are the global elastic stiffness matrix and geometric stiffness matrix, $\{\boldsymbol{\delta}\}$ is the buckling mode shape vector and λ is the critical buckling load parameter, respectively.

3.2. Dynamic analysis

In the case of vibration analysis the governing equations of motion are solved as an eigen-value problem. The mass matrix can be determined directly from the kinetic energy. This is computed in the finite element

framework by employing the Hamilton's Principle. Finally, the element mass matrix is expressed in the natural coordinate system as Eq. (28),

$$\mathcal{M}_e = \sum_{1}^{n_t} \int_A \mathbf{S}^\top \mathcal{M}_I \mathbf{S} \rho_k \; dA \tag{28}$$

where, ρ_k represents the density of composite lamina. The value of **S** matrix is computed using the shape functions. The inertia matrix ($\mathcal{M}_I$) for the k-th layer is calculated as,

$$\mathcal{M}_I = \begin{bmatrix} z_k & 0 & 0 & \frac{z_k^2}{2} & 0 & c\frac{z_k^4}{4} & 0 & \phi_1^{(k)} & 0 \\ & z_k & 0 & 0 & \frac{z_k^2}{2} & 0 & c\frac{z_k^4}{4} & 0 & \phi_2^{(k)} \\ & & z_k & 0 & 0 & 0 & 0 & 0 & 0 \\ & & & \frac{z_k^3}{3} & 0 & c\frac{z_k^5}{5} & 0 & z_k^2\phi_1^{(k)} & 0 \\ & \text{Symm.} & & & \frac{z_k^3}{3} & 0 & c\frac{z_k^5}{5} & 0 & z_k^2\phi_2^{(k)} \\ & & & & & c^2\frac{z_k^7}{7} & 0 & cz_k^4\phi_1^{(k)} & 0 \\ & & & & & & c^2\frac{z_k^7}{7} & 0 & cz_k^4\phi_2^{(k)} \\ & & & & & & & \int_{z_{k-1}}^{z_k} (\phi_1^{(k)})^2 dz & 0 \\ & & & & & & & & \int_{z_{k-1}}^{z_k} (\phi_2^{(k)})^2 dz \end{bmatrix} \tag{29}$$

The eigenvalues and eigenvectors obtained from the solution are the natural frequencies and corresponding mode shapes of the laminate. In this work an undamped free vibration is performed. The equations of motion for undamped free vibration are given by Eq. (30),

$$\omega^2[\mathcal{M}]\{\boldsymbol{\delta}\} = [\mathbf{K}]\{\boldsymbol{\delta}\} \tag{30}$$

where, $[\mathcal{M}]$ and $[\mathbf{K}]$ are global mass and stiffness matrices, respectively. The relative displacement mode corresponding to the natural frequency is represented as $\{\boldsymbol{\delta}\}$.

The global elastic stiffness matrix is used in both stability and dynamic analyses. In the case of stability analysis, the global geometric stiffness matrix and global geometric stiffness matrix are employed to evaluate the critical buckling load. On the other hand, in the dynamic analysis global mass and global elastic stiffness matrices are utilised to solve the free vibration problem and obtain the natural frequency. All the numerical studies presented in this article are performed using MATLAB. The numerical implementation of each of the above-mentioned problems is schematically shown in Figure 2.

4. Numerical verification

At first the proposed framework is numerically verified with published data. Numerical specimens of two cross-ply laminates—$[0^\circ/90^\circ/0^\circ]$ and $[0^\circ/90^\circ]_s$, are employed for this purpose. In this article these laminates are referred to as three-layered and four-layered laminates, respectively. The composite laminate is assumed to have the transverse elastic modulus (E_2) of 1 GPa and density of 1 kg/m^3. The Poisson's ratio along all three directions are assumed to be 0.25, i.e. $\nu_{12} = \nu_{13} = \nu_{23} = 0.25$. The longitudinal elastic modulus (E_1) of the composite is obtained based on the E_1/E_2 ratio. In this study five different E_1/E_2 ratio are considered, such as, 3, 10, 20, 30 and 40. The shear moduli of the composite are also considered as functions of the transverse elastic modulus, $G_{12} = G_{13} = 0.6E_2$; $G_{23} = 0.2E_2$. In this numerical verification several types of boundary conditions are considered. In the first case it is assumed that the laminate is simply-supported along all four edges and denoted by SSSS. In the second case all four edges are assumed to be clamped and referred to as CCCC. A third case considered simply-supported and clamped boundaries in adjacent alternate edges. Finally, clamped and free boundary conditions are assumed in

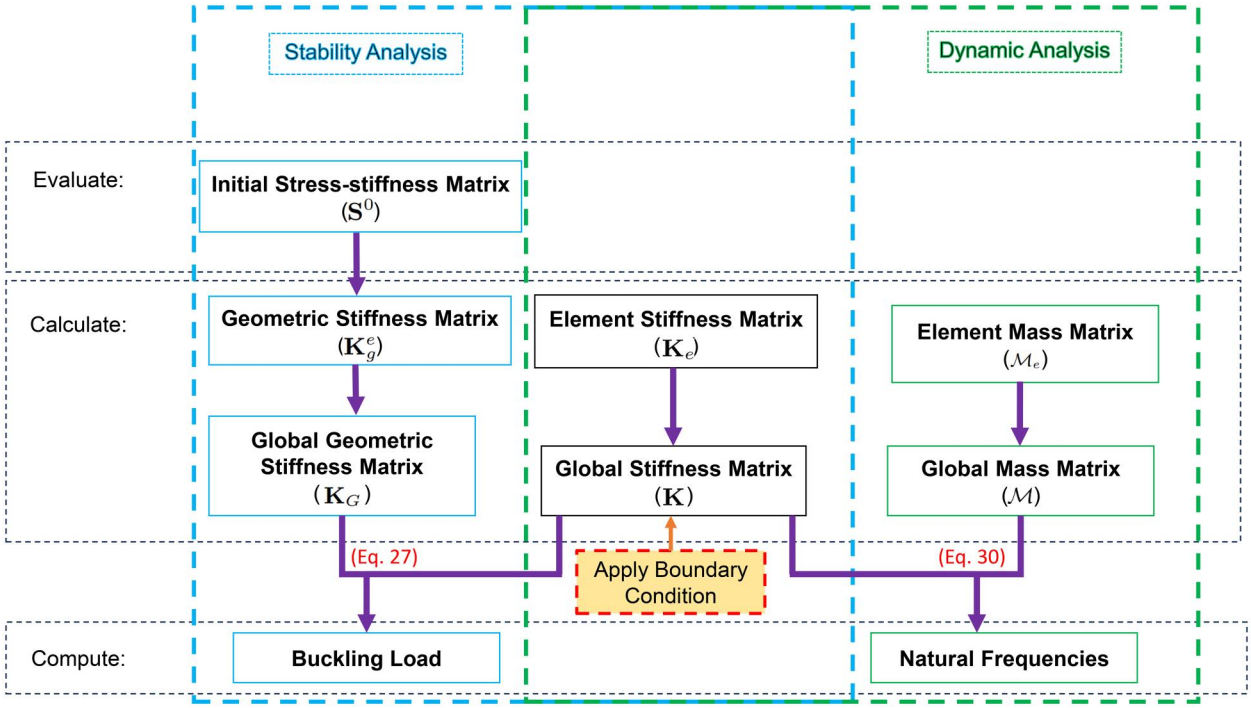

Figure 2. Flowchart showing numerical implementation to solve stability and dynamic problems.

Table 1. Boundary conditions.

Boundary condition	Edges along x_1	Edges along x_2
SSSS	$v_2 = v_3 = 0$ $\theta_2 = \eta_2 = \psi_2 = 0$	$v_1 = v_3 = 0$ $\theta_1 = \eta_1 = \psi_1 = 0$
CCCC	$v_1 = v_2 = v_3 = \theta_1 = \theta_2 = \eta_1 = \eta_2 = \psi_1 = \psi_2 = 0$	
SCSC	$v_2 = v_3 = 0$ $\theta_2 = \eta_2 = \psi_2 = 0$	$v_1 = v_2 = v_3 = \theta_1 = \theta_2 = 0$ $\eta_1 = \eta_2 = \psi_1 = \psi_2 = 0$
CFCF	$v_1 = v_2 = v_3 = \theta_1 = \theta_2 = 0$ $\eta_1 = \eta_2 = \psi_1 = \psi_2 = 0$	–

alternate adjacent laminate edges. The last two cases of boundary conditions are denoted as SCSC and CFCF, respectively. The kinematic boundary conditions employed in both the cases are given in Table 1.

The numerical verification of the proposed formulation is evaluated by performing stability and dynamic analyses. In the stability analysis evaluation of the critical buckling strength is the parameter of interest. In the dynamic analysis the problem is solved for a free-vibration case yielding multiple natural frequencies and mode shapes. The verification is intended to evaluate the prediction of natural frequencies of laminates. The stability and dynamic analyses are described in Section 4.1 and Section 4.2, respectively.

4.1. Stability analysis

Simply supported square cross-ply laminates are analysed in this section for the numerical verification. At first a mesh convergence study is performed to obtain mesh objectivity in the prediction. The square plate is discretised with uniform mesh along adjacent edges. In this study five different discretizations are evaluated. In those five discretisation cases the number of mesh along each edge is varied as 8, 10, 12, 16 and 20. The relative percentage (ε) error in the numerical solution of a laminate is compared to the reference 3D solution and calculated as,

$$\varepsilon(\%) = \frac{\lambda_{cr}^{3D} - \lambda_{cr}}{\lambda_{cr}^{3D}} \times 100 \tag{31}$$

where, λ_{cr}^{3D} represents the normalised critical buckling strength obtained from the 3D elastic solution [3] and λ_{cr} is the normalised critical buckling strength obtained from RHZT or RFZT formulation by changing total number of elements. The normalised critical buckling strength [3] is obtained using the following equation,

$$\lambda_{cr} = \lambda \frac{a^2}{E_2 h^3} \tag{32}$$

where, λ is the buckling strength obtained from the present analysis. h is the total thickness of the plate

and a indicates the length of plate along $\mathbf{x_1}$ direction. The uniaxial compression is verified using a three-layer and a four-layer square laminate and are described in Section 4.1.1. A constant span to thickness ratio (a/h) of 10 is used under uniaxial compression. Following the verification under uniaxial compression the biaxial compression case is provided in Section 4.1.2. In the biaxial compression case three different span to thickness ratios (10, 20 and 50) are evaluated.

4.1.1. Verification: Critical buckling strength under uniaxial compression

First the numerical verification is performed for the three layer laminate. The normalised (non-dimensional) critical buckling strengths under uniaxial compression are computed based on the proposed ZZ-based formulations, i.e. RFZT and RHZT. The normalised critical buckling strength are compared with 3D elastic solution (as a reference) from published literature [3]. Additionally, the prediction of the proposed formulation is evaluated with published data from non-ZZ-based model-based shell theories. The numerical solution appears to converge with 256 elements (discretisation of 16×16). The verification study for three-layered laminate subjected to uniaxial compression is shown in Table 2. In this table the results with a discretisation of 16×16 are shown in bold fonts. In in Table 2 it can be observed that the proposed RHZT and RFZT formulations have the capability to provide comparable prediction with the 3D elastic results with 0.4% and 3.5% accuracy, respectively. This clearly shows that RHZT is capable of predicting critical buckling strength with better accuracy as compared to the first-order theory (RFZT).

Next, the formulation is verified with the four-layer cross-ply laminate. Same material properties, boundary conditions and a/h ratio are used as in the three-layer laminate case. The results of four-layer laminate are presented in Table 3. Similar to the three-layer laminate, the critical buckling strengths tend to converge at a discretisation of 16×16. Due to lack of

Table 2. Non-Dimensional buckling strengths of $[0^\circ/90^\circ/0^\circ]$ square laminate under uniaxial compression.

		E_1/E_2									
		3		10		20		30		40	
Model	Mesh	λ_{cr}	ε (%)	λ_{cr}	ε (%)	λ_{cr}	ε (%)	λ_{cr}	ε (%)	λ_{cr}	ε (%)
RHZT	8×8	5.3187	0.27	9.7455	0.17	14.9782	0.27	19.2544	0.26	22.8088	0.31
	10×10	5.3185	0.27	9.7435	0.19	14.9776	0.28	19.2509	0.27	22.8065	0.32
	12×12	5.3185	0.27	9.7423	0.20	14.9764	0.28	19.2491	0.28	22.8065	0.32
	16×16	**5.3184**	**0.26**	**9.7422**	**0.20**	**14.9748**	**0.29**	**19.2470**	**0.30**	**22.8019**	**0.34**
	20×20	5.3184	0.26	9.7422	0.20	14.9748	0.29	19.2470	0.30	22.8019	0.34
RFZT	8×8	5.1596	2.73	9.4526	3.17	14.5276	3.27	18.6752	3.26	22.1223	3.31
	10×10	5.1594	2.73	9.4507	3.19	14.5270	3.28	18.6718	3.27	22.1200	3.32
	12×12	5.1593	2.73	9.4495	3.20	14.5258	3.28	18.6700	3.28	22.1200	3.32
	16×16	**5.1593**	**2.74**	**9.4494**	**3.20**	**14.5242**	**3.29**	**18.6679**	**3.30**	**22.1154**	**3.34**
	20×20	5.1593	2.74	9.4494	3.20	14.5242	3.29	18.6679	3.30	22.1154	3.34
3D Elasticity [3]		5.3044	–	9.7621	–	15.0191	–	19.3040	–	22.8807	–
Anish *et al.* [25]		5.3142	0.18	9.6982	0.65	14.6927	2.17	18.6343	3.47	21.8415	4.54
Reddy and Phan (HSDT) [16]		5.3933	1.68	9.9406	1.83	15.2980	1.86	19.6740	1.92	23.3400	2.01
Reddy and Phan (FSDT) [16]		5.3931	1.67	9.9625	2.05	15.3510	2.21	19.7560	2.34	23.4530	2.50

Table 3. Non-Dimensional buckling strengths of $[0^\circ/90^\circ]_s$ square laminate under uniaxial compression.

		E_1/E_2									
		3		10		20		30		40	
Model	Mesh	λ_{cr}	ε (%)	λ_{cr}	ε (%)	λ_{cr}	ε (%)	λ_{cr}	ε (%)	λ_{cr}	ε (%)
RHZT	8×8	5.3218	0.04	9.8367	0.29	15.1767	0.49	19.5544	0.64	23.2337	0.77
	10×10	5.3216	0.04	9.8364	0.28	15.1762	0.49	19.5538	0.64	23.2331	0.77
	12×12	5.3215	0.03	9.8363	0.28	15.1760	0.49	19.5536	0.64	23.2329	0.77
	16×16	**5.3215**	**0.03**	**9.8363**	**0.28**	**15.1759**	**0.49**	**19.5535**	**0.64**	**23.2327**	**0.76**
	20×20	5.3215	0.03	9.8362	0.28	15.1759	0.49	19.5535	0.64	23.2327	0.76
RFZT	8×8	5.4889	3.18	9.9741	1.69	15.1117	0.06	19.2273	1.04	22.6441	1.79
	10×10	5.4887	3.18	9.9738	1.68	15.1113	0.06	19.2268	1.04	22.6435	1.79
	12×12	5.4887	3.18	9.9737	1.68	15.1111	0.06	19.2266	1.04	22.6433	1.79
	16×16	**5.4886**	**3.17**	**9.9736**	**1.68**	**15.1110**	**0.06**	**19.2265**	**1.04**	**22.6432**	**1.79**
	20×20	5.4886	3.17	9.9736	1.68	15.1110	0.06	19.2265	1.04	22.6432	1.79
Anish *et al.* [25]		5.3197	–	9.8087	–	15.1025	–	19.4295	–	23.0565	–
Nguyen-Van *et al.* [8]		5.3210	0.02	9.8090	0.01	15.0640	0.25	19.3390	0.47	22.9120	0.63
Liu *et al.* [53]		5.4120	1.74	10.0130	2.08	15.3090	1.37	19.7780	1.79	23.4120	1.54

published data performing 3D elastic analysis using four-layer laminate, results from Anish *et al.* [25] are used as the reference of the verification. It can be noted that the predictions from the present RHZT formulation are in good agreement with the relevant published results.

4.1.2. Verification: Critical buckling strength under biaxial compression

The verification under biaxial loading is performed using the three-layer square laminate with all edges simply supported (SSSS boundary condition). The span to thickness ratios (a/h) are considered to be 10, 20 and 50 and the E_1/E_2 ratios are 10 and 20. Discretisation of 16×16 is only used for verification under biaxial compression. The critical buckling strengths obtained from the proposed formulation are compared with those published data [25] as reference. Additionally, the performance of the proposed model is evaluated with the results by Vescovini and Dozio [44]. The results shown in Table 4 demonstrate the accuracy of the proposed RHZT formulation in predicting the critical buckling strengths of laminated composites.

4.2. Dynamic analysis

In this section the proposed formulation is numerically verified for free-vibration problem, also referred to as modal analysis. The mesh objectivity is ensured using a mesh convergence study for a simply-supported square cross-ply laminate. The natural frequencies are reported six different the span-to-thickness ratio (a/h) of the laminate. The normalised value of fundamental frequency [12] obtained from the present formulation is calculated by using the following equation:

$$\omega^* = \frac{\omega a^2}{h}\sqrt{\frac{\rho}{E_2}} \tag{33}$$

where, ω is the calculated fundamental frequency and ρ is the density. First, the predicted fundamental frequencies obtained using proposed formulation are verified with data from published literature [12]. This reference data is obtained using the *p*-Ritz method.

4.2.1. Verification: Natural frequencies of laminate

First, the four-layered square laminate with simply supported boundary conditions is employed for numerical verification. Similar to the stability analysis, the dynamic analysis leads to the converged solution

Table 4. Non-Dimensional buckling strengths of $[0^\circ/90^\circ]_s$ square laminate under biaxial compression.

		a/h					
		10		20		50	
E_1/E_2	Model	λ_{cr}	ε (%)	λ_{cr}	ε (%)	λ_{cr}	ε (%)
10	RHZT	4.8704	0.54	5.4984	0.17	5.7068	0.03
	RFZT	4.9029	1.21	5.5071	0.33	5.7101	0.03
	Anish et al. [25]	4.8441	–	5.4890	–	5.7084	–
	Vescovini and Dozio [44]	4.9095	1.35	5.5082	0.35	5.7063	0.04
20	RHZT	8.0049	1.24	9.9523	1.32	10.7116	0.07
	RFZT	8.0783	2.17	9.9718	1.12	10.7233	0.18
	Anish et al. [25]	7.9066	–	10.0852	–	10.7040	–
	Vescovini and Dozio [44]	8.6820	9.81	10.8768	7.85	11.7320	9.60

Table 5. Normalised fundamental frequency of square $[0^\circ/90^\circ]_s$ laminate with varying a/h ratio.

		a/h											
		5		10		20		25		50		100	
Model	Mesh	ω^*	ε (%)	ω^*	ε (%)	ω^*	ε (%)	ω^*	ε (%)	ω^*	ε (%)	ω^*	ε (%)
RHZT	8×8	10.331	4.83	14.632	3.38	17.631	0.16	18.179	0.59	19.022	1.87	19.257	2.23
	10×10	10.331	4.83	14.632	3.38	17.630	0.16	18.178	0.59	19.021	1.86	19.256	2.23
	12×12	10.331	4.83	14.632	3.38	17.630	0.16	18.178	0.59	19.021	1.86	19.255	2.23
	16×16	**10.330**	**4.83**	**14.631**	**3.38**	**17.630**	**0.16**	**18.178**	**0.59**	**19.021**	**1.86**	**19.255**	**2.23**
	20×20	10.330	4.83	14.631	3.38	17.630	0.16	18.178	0.59	19.020	1.86	19.255	2.23
RFZT	8×8	10.878	0.21	15.209	0.44	17.694	0.20	18.095	0.13	18.682	0.05	18.839	0.02
	10×10	10.878	0.21	15.209	0.43	17.693	0.20	18.095	0.13	18.681	0.04	18.838	0.01
	12×12	10.878	0.21	15.209	0.43	17.693	0.20	18.094	0.13	18.681	0.04	18.838	0.01
	16×16	**10.878**	**0.21**	**15.209**	**0.43**	**17.693**	**0.20**	**18.094**	**0.13**	**18.681**	**0.04**	**18.838**	**0.01**
	20×20	10.878	0.21	15.209	0.43	17.693	0.20	18.094	0.12	18.681	0.04	18.838	0.01
Liew [12]		10.855	–	15.143	–	17.658	–	18.072	–	18.673	–	18.836	–
Reddy and Phan [16]		10.989	1.24	15.269	0.83	17.667	0.05	18.049	0.13	18.462	1.13	18.756	0.42
Cho *et al.* [30]		10.673	1.68	15.066	0.51	17.535	0.70	18.054	0.10	18.670	0.02	18.835	0.01

with 16×16 Discretisation. The mesh convergence study and numerical verification based on the normalised fundamental frequency are given in Table 5. Additionally, the results obtained based on ZZ-theory are compared with published data that employed HSDT [16] and higher-order individual layer theory [30]. It can be seen that the results obtained using proposed formulation are in closer agreement with the reference data. It is to be noted that the span-to-thickness ratio (a/h) has a considerable effect on the fundamental frequency of plates at lower a/h ratios. At higher a/h ratios ($a/h > 25$), the influence on the fundamental frequency is insignificant. However, the error calculated from the solution using RHZT is higher compared to the RHZT. This is due to the fact that higher-order theory considers additional degrees-of-freedom in each element which makes the element more flexible than those using first-order approximation.

Finally, the three-layered cross-ply square laminate is analysed to estimate the first five modal frequencies under different boundary conditions. For each boundary condition the natural frequencies are estimated due to four different span-to-thickness ratios (a/h). The first five normalised natural frequencies are compared with data from published literature [12] and given in Table 6. This numerical verification ensures that the proposed model has the capability to predict natural frequencies with significant accuracy.

Table 6. Normalised natural frequencies of $[0^\circ/90^\circ/0^\circ]$ square laminate with different boundary conditions.

			Mode sequence				
Boundary	a/h	Model	I	II	III	IV	V
SSSS	5	RHZT	9.9329	15.1754	21.7003	24.6384	25.7845
		RFZT	10.4728	15.9741	22.1948	24.5097	25.3353
		Liew [12]	10.2560	16.4626	21.1083	24.7924	26.0965
	10	RHZT	14.2556	21.1860	35.0776	37.1675	40.7378
		RFZT	14.9126	21.9336	36.4975	38.3663	41.8968
		Liew [12]	14.7419	22.1356	36.8547	37.2371	41.0238
	20	RHZT	17.4539	25.1768	42.1178	55.6697	57.0349
		RFZT	17.5778	25.3051	42.5588	55.9894	59.6597
		Liew [12]	17.5156	25.3631	43.1184	55.2292	58.9703
	1000	RHZT	19.3355	27.0313	46.3139	71.6658	75.6774
		RFZT	18.8913	26.9486	46.2969	71.6286	75.6532
		Liew [12]	18.9053	26.9583	46.2431	71.6719	75.6156
CCCC	5	RHZT	12.6939	17.9464	21.8872	25.8062	26.3023
		RFZT	13.0267	18.6220	22.2532	26.8680	26.9253
		Liew [12]	12.6901	18.9538	21.9730	26.2106	27.7887
	10	RHZT	20.7466	28.1314	40.2180	44.4984	44.7698
		RFZT	21.7203	29.3755	41.5349	45.4145	46.2986
		Liew [12]	21.1483	29.6578	39.7026	44.0287	45.1045
	20	RHZT	30.3852	39.8152	57.6348	65.4973	70.3976
		RFZT	31.7488	40.1177	57.2977	67.0787	72.8800
		Liew [12]	31.2559	40.0308	58.1799	66.1929	71.2781
	1000	RHZT	42.0161	50.1570	69.9143	101.5622	111.8178
		RFZT	41.9379	50.2740	70.0605	101.6017	112.0340
		Liew [12]	41.8514	50.2639	69.9454	101.3953	111.7397
SCSC	5	RHZT	11.1910	17.5419	22.2846	25.5091	26.4880
		RFZT	11.5732	17.2720	22.7141	25.7260	26.1644
		Liew [12]	11.8055	18.4744	21.8703	26.1364	27.5176
	10	RHZT	16.3447	25.6133	37.2626	41.2411	42.3107
		RFZT	17.2168	25.6550	39.0776	42.0176	44.1704
		Liew [12]	16.7537	26.9783	38.0675	42.4564	43.7747
	20	RHZT	19.7386	31.8235	52.7413	55.0812	63.3474
		RFZT	20.4627	32.5198	53.9307	56.3719	64.5489
		Liew [12]	19.6615	32.0920	53.2602	55.9854	62.2121
	1000	RHZT	21.2741	34.5129	59.3671	72.4189	79.2202
		RFZT	21.1918	34.5069	59.5545	72.3652	79.3327
		Liew [12]	21.1055	34.6545	59.4726	72.3824	78.9629
CFCF	5	RHZT	4.2153	4.4195	9.3275	13.8967	13.0467
		RFZT	4.8457	4.5941	9.6505	14.2719	14.5398
		Liew [12]	4.1207	4.4089	9.8907	13.3750	13.8687
	10	RHZT	5.1458	5.8375	11.9379	22.1136	22.9814
		RFZT	5.8246	5.9368	11.1372	23.0848	23.7095
		Liew [12]	5.4733	6.0012	11.9510	22.1356	22.7178
	20	RHZT	6.0148	6.5904	12.3578	27.4661	31.2222
		RFZT	6.5486	6.5383	12.3356	27.6860	32.3002
		Liew [12]	6.0697	6.7603	13.0097	28.6505	31.5897
	1000	RHZT	6.4528	7.0844	13.5062	30.0306	39.8101
		RFZT	6.3988	7.0164	13.6932	30.0473	39.9007
		Liew [12]	6.3122	7.1027	13.5633	30.0687	39.5514

5. Numerical examples: Analysis of hybrid laminates

In the case of composite laminates, the concept of hybridisation involves replacing layups of weaker fibre material with stronger fibre material. To enhance structural performance often Carbon Fibre Reinforced Polymer (CFRP) composite layups are incorporated in Glass Fibre Reinforced Polymer (GFRP) laminates to make it a Hybrid Fibre Reinforced Polymer (HFRP) composite laminate. Therefore, in a hybrid laminate, during manufacturing individual GFRP layups are replaced with CFRP layups of same thickness. The "percentage of hybridisation" is defined as a ratio of the volume of CFRP content to the total volume of the laminate.

The performance of a HFRP laminate is evaluated with respect to laminates of pure GFRP laminates of equivalent volume. It is to be noted that replacement of GFRP layups with CFRP layups (with same fibre orientation) would lead to change in the total number of layups. In this study, following example laminates with two different layup sequences are considered. The black and magenta colours in Figure 3 indicate CFRP and GFRP layups, respectively.

- HFRP-1: A six-layered laminate with layup sequence $[0^\circ/0^\circ/90^\circ]_s$
- HFRP-2: An eight-layered laminate with layup sequence $[0^\circ/0^\circ/90^\circ/90^\circ]_s$

Following the numerical verification, the proposed framework is employed to investigate the response of HFRP laminates. The mechanical properties of the CFRP and GFRP composites used in this study are given in Table 7.

At first four-layered GFRP laminates with equal thickness are analysed, followed by the HFRP laminates. In both the examples, parametric studies are performed based on the laminate geometry, laminate boundary conditions and percentage hybridisation. Following parameters are considered for the laminate geometry and boundary conditions.

i. Aspect ratio (a/b): 0.25, 0.50, 0.75, and 1.00,
ii. Span to thickness ratio (a/h): 10, 20, 50, 100, and
iii. Boundary conditions: SSSS and CCCC

The stability and dynamic analyses of hybrid laminates are discussed in Section 5.1 and Section 5.2, respectively.

5.1. Stability analysis

At first, square-shaped hybrid laminates are studied for the effect of change in the percentage of hybridisation. Next, keeping percentage of hybridisation as constant, the effect of hybridisation on critical

Table 7. Mechanical properties of CFRP and GFRP.

Elastic parameters	CFRP	GFRP	Unit
E_1	137.0	41.6	GPa
E_2	12.4	8.78	GPa
ν_{12}	0.33	0.274	–
ν_{13}	0.33	0.274	–
ν_{23}	0.214	0.314	–
G_{12}	4.66	3.45	GPa
G_{13}	4.66	3.45	GPa
G_{23}	54.6	15.8	GPa
Density	1710	2065	kg/m^3

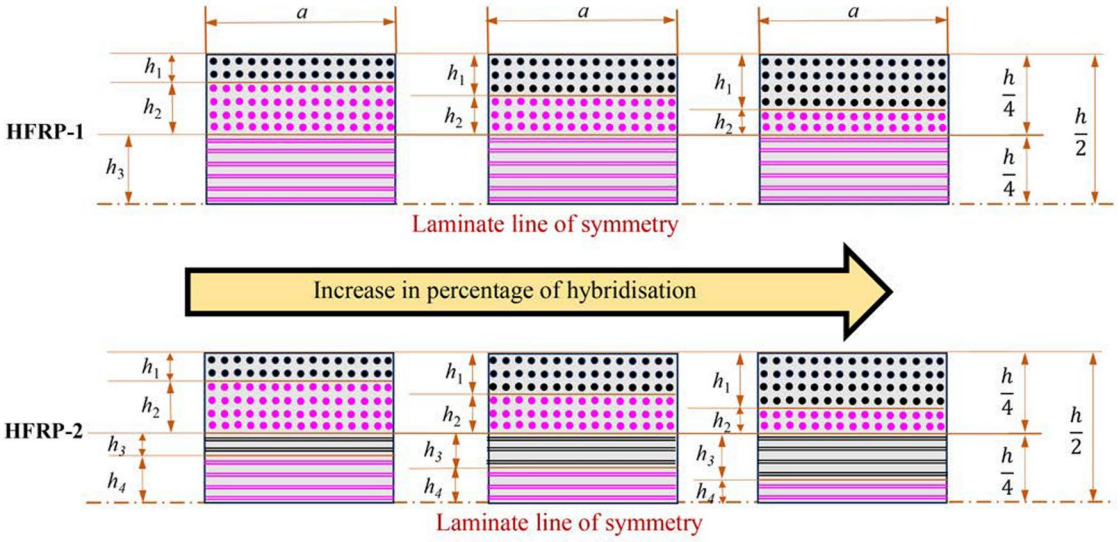

Figure 3. Schematic representation showing cross-sections of two HFRP laminates.

buckling strength is evaluated based on the geometric parameters and boundary conditions.

5.1.1. Effect of hybridisation on critical buckling strength

The objective of this study is to understand the effect of hybridisation on critical buckling strength of square-shaped HFRP laminate. The HFRP-1 and HFRP-2 laminates are analysed by increasing the percentage of hybridisation from 0% up to 50%. The variation of the buckling strengths for HFRP-1 and HFRP-2 are shown in Figures 4 and 5, respectively. It is noted that both the HFRP laminates possess nearly similar buckling strength while other parameters remain constant. Additionally, the buckling strength of thicker plates are significantly higher compared to thinner plates.

To quantify the improvement in buckling strength the critical buckling strengths are normalised by using the following expression (as a modified form of Eq. (32)):

$$\lambda_{cr} = \lambda \frac{a^2}{E_2^{\mathrm{GFRP}} h^3} \tag{34}$$

Next, the percentage increase ($\mathcal{I}_b$) in the normalised critical buckling strength of HFRP laminates is determined as:

$$\mathcal{I}_b(\%) = \frac{\lambda_{cr}^{HFRP} - \lambda_{cr}^{GFRP}}{\lambda_{cr}^{GFRP}} \times 100 \tag{35}$$

A comparison showing the percentage increase of critical buckling strengths of HFRP and pure GFRP laminates are shown in Figures 6 and 7. Laminates with simply-supported boundary conditions demonstrate a similar trend under uniaxial and biaxial loading. It is apparent that HFRP-1 laminates reach much higher percentage increase compared to HFRP-2 laminates. On the other hand, clamped laminates demonstrate a different behaviour. It can be seen that with HFRP-1 laminate an improvement up to 150% be achieved, whereas with HFRP-2 laminate improvement observed up to 120% for same percentage of hybridisation. The buckling strength of HFRP-1 is higher than HFRP-2 laminate as larger quantity of carbon fibre is aligned in loading direction in HFRP-1. Additionally, for very thick laminates (i.e. a/h value of 10) under uniaxial compression with clamped boundary condition, the improvement in buckling strength is significantly less. During biaxial loading condition with clamped boundary condition, improvements in both the HFRP laminates are very similar performance. Therefore, it can be concluded that the

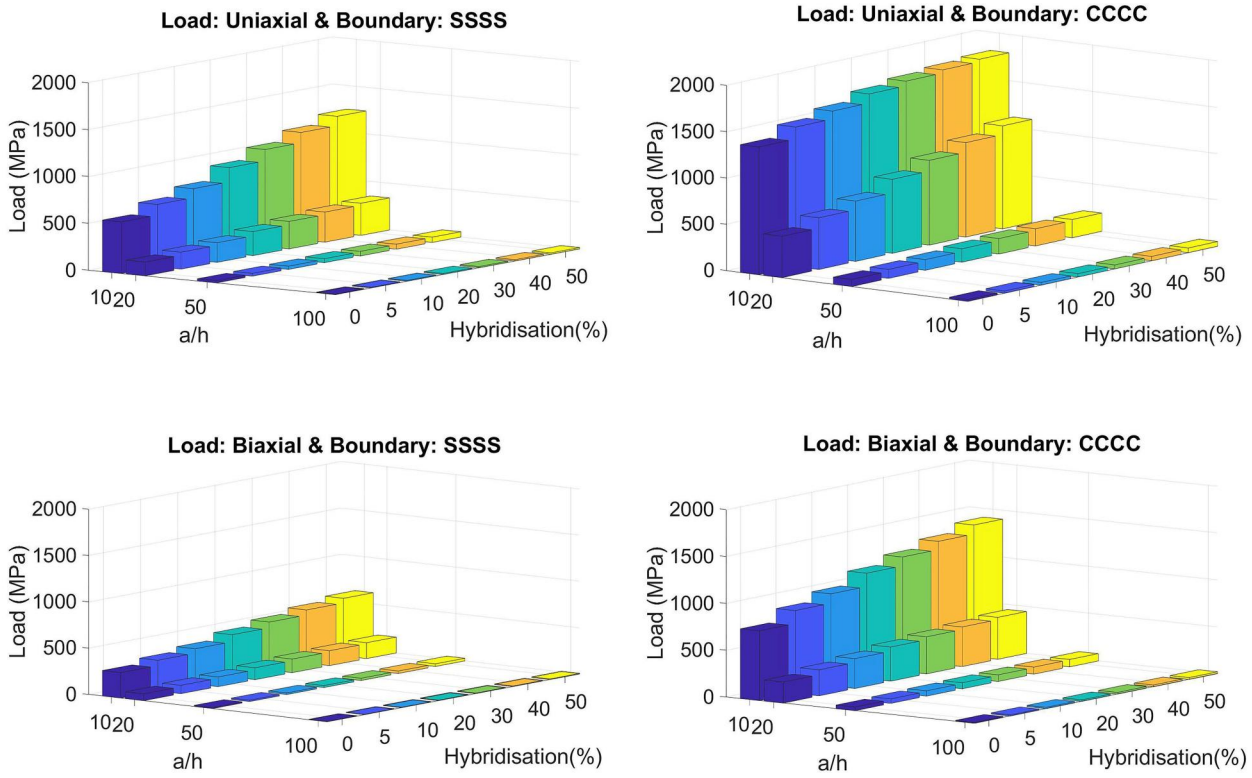

Figure 4. Variation of buckling strengths of HFRP-1 laminate due to hybridisation and a/h ratio.

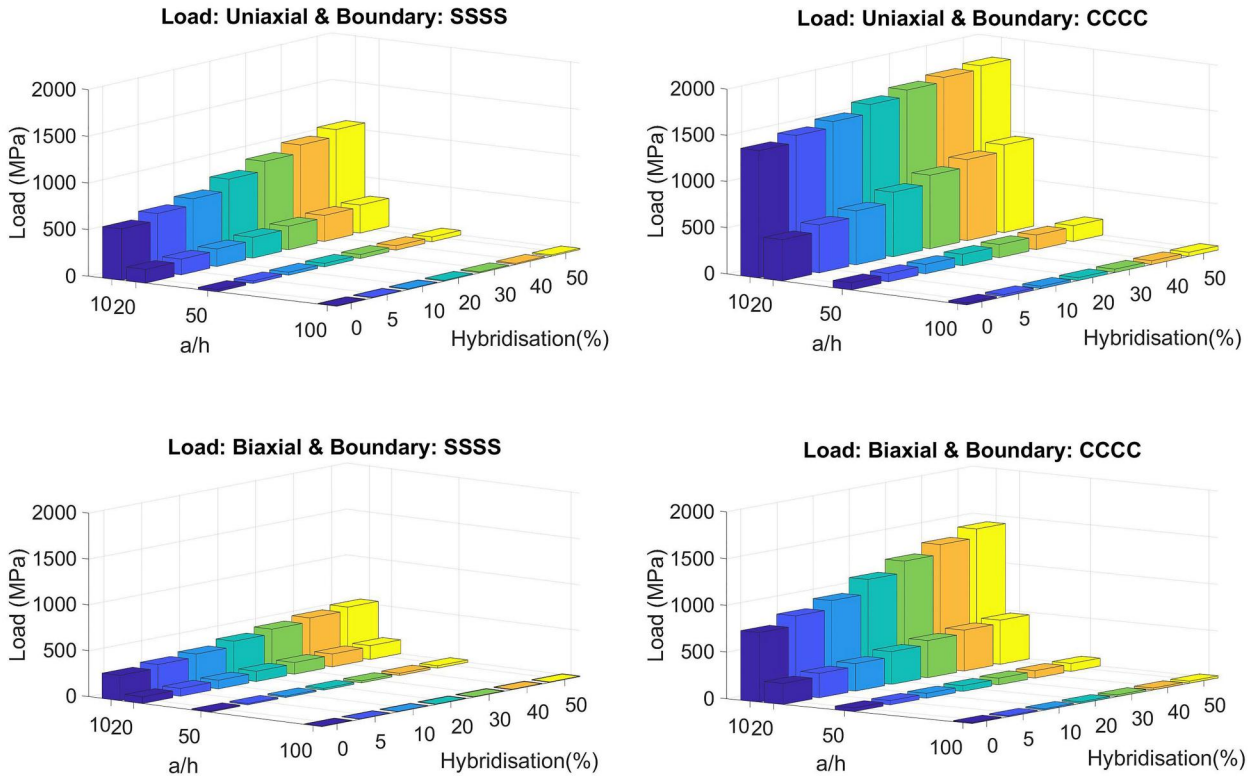

Figure 5. Variation of buckling strengths of HFRP-2 laminate due to hybridisation and a/h ratio.

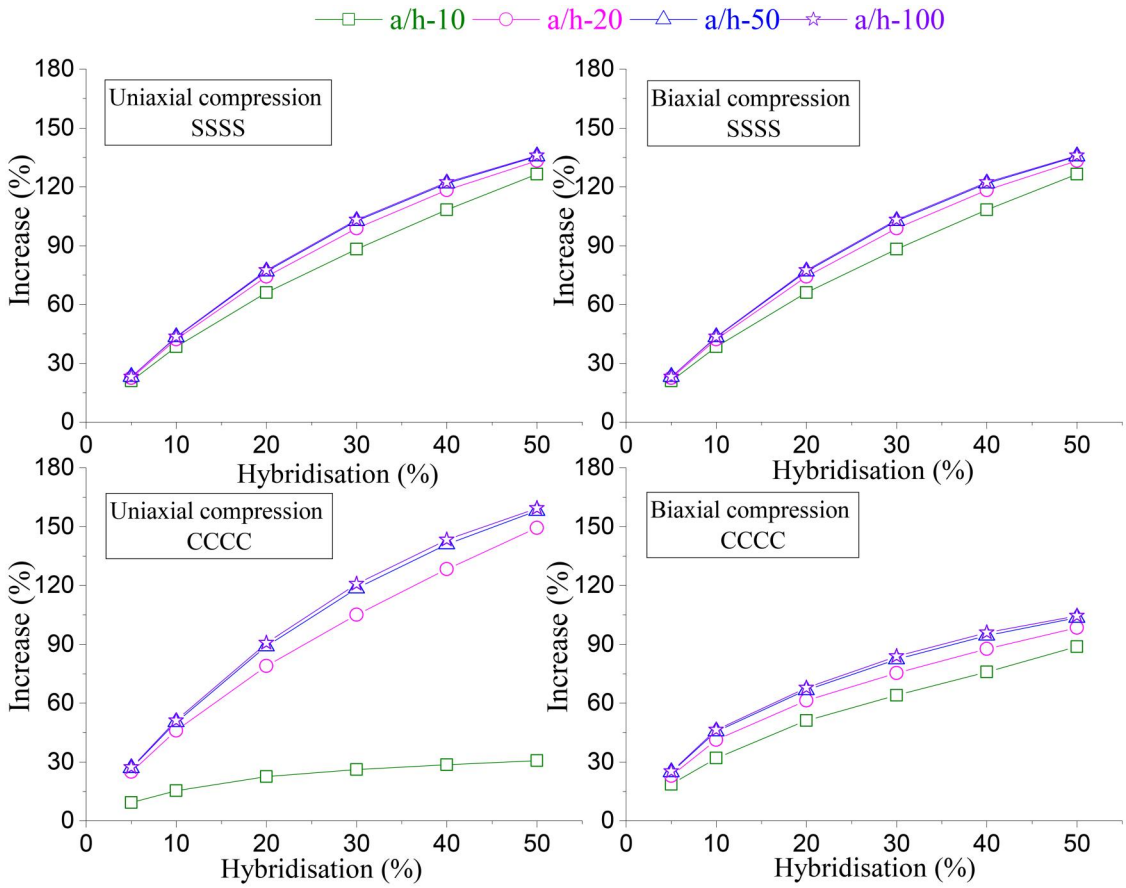

Figure 6. Percentage increase in critical buckling strength of HFRP-1 laminate to GFRP laminate.

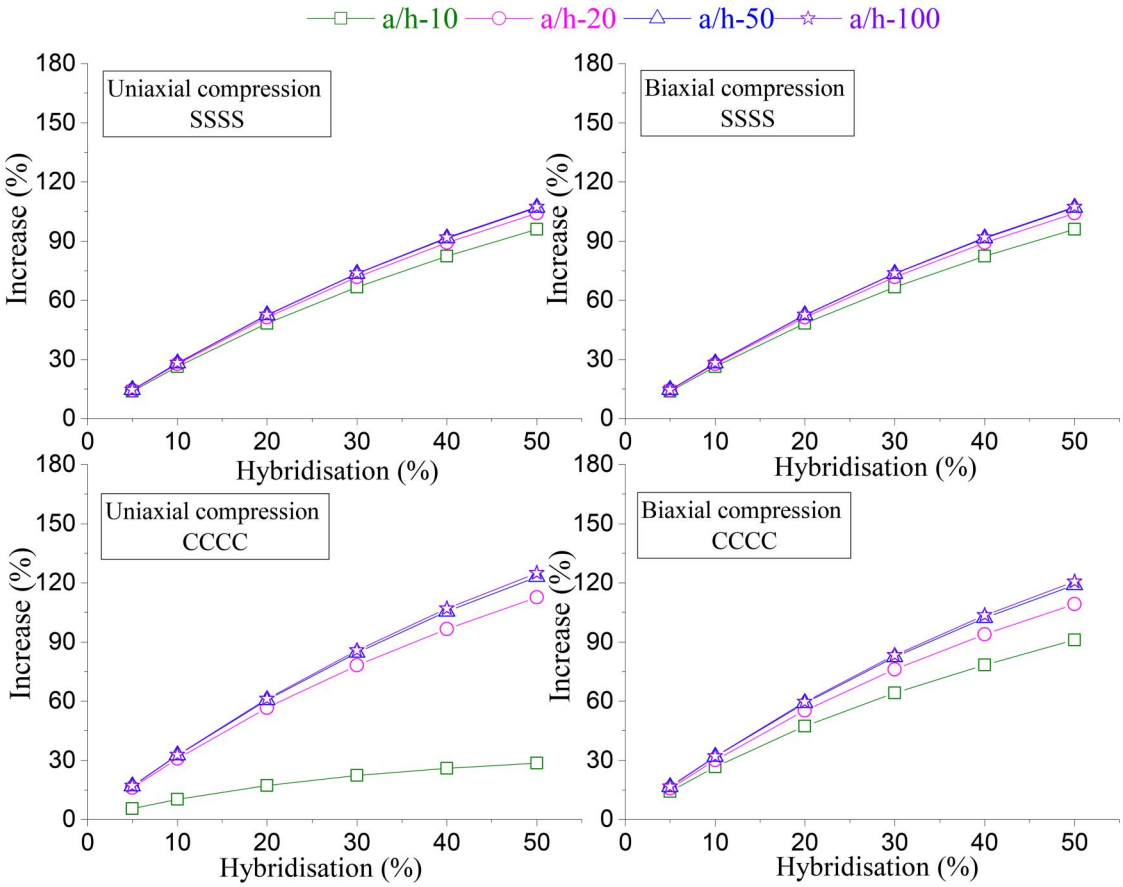

Figure 7. Percentage increase in critical buckling strength of HFRP-2 laminate to GFRP laminate.

effect of laminate configuration is insignificant when the effect of hybridisation is studied.

5.1.2. Effect of aspect ratio on buckling analysis of hybrid laminates

Next, the effect of laminate aspect ratio is studied considering 50% fibre hybridisation. Similar to the previous analysis the specimens are studied for both uniaxial and biaxial compression. The assumption of equal layup thickness for each material remains valid, too. The strength comparison performed in this section is with various geometric parameters, i.e. aspect ratio and span to thickness ratio. The percentage increase in the normalised critical buckling strength is given in Tables 8 and 9. Under uniaxial compression the normalised critical buckling strength of HFRP-1 and HFRP-2 laminates with simply-supported boundary condition increases approximately 1.3 and 1.5 times, respectively, with the increase in the aspect ratio. In the case of clamped boundary condition the increase in aspect ratio of thinner laminates leads to 1.2 and 1.3 times, respectively. During biaxial compression, even with low aspect ratio, the hybrid laminates cannot achieve the same buckling strength as under uniaxial loading. This is attributed to the lower buckling resisting capacity of the layups along the transverse direction. Additionally, loss in critical buckling strength is observed in the thinner laminates. Laminates with the clamped boundary condition demonstrate approximately four times higher buckling strength under uniaxial compression. It is observed that under biaxial loading with clamped boundary condition increase in the laminate aspect ratio affects the increase in buckling strength for HFRP-1 laminate. It is evident that the addition of the CFRP layup in the transverse direction of the HFRP-2 laminate contributed towards the strength enhancement. It is to be noted that under the uniaxial compression, $\mathcal{I}_b$ in HFRP laminates decreases with the increase of aspect ratio. On the other hand, the $\mathcal{I}_b$ increases with increase of span-to-thickness ratio (a/h). For thinner plates the increase in the buckling strength reached up to a certain limit. Beyond that limit $\mathcal{I}_b$ will become constant. This orthotropic change in the buckling load carrying capacity is due to the presence of high strength CFRP along the x_1 direction. However, under biaxial compression the effect of a/b becomes insignificant during biaxial compression. It is observed that as the a/b increases, the biaxial critical buckling strength increases for both GFRP and HFRP. As a result, the percentage increase in the critical buckling strength remains constant for biaxial compression.

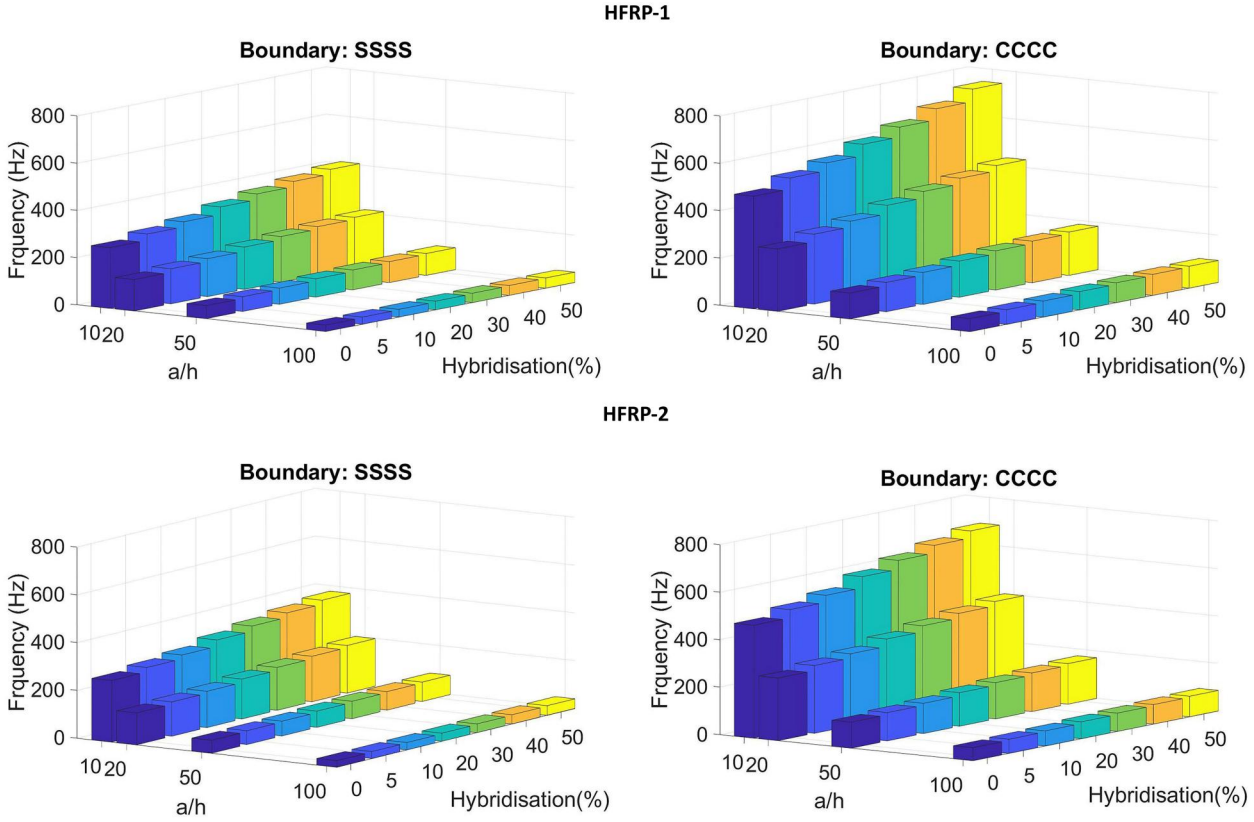

Figure 8. First natural frequency of HFRP laminates for change of hybridisation and a/h ratio.

Table 8. Percentage increase ($\mathcal{I}_b$) in normalised critical buckling strength of HFRP-1.

Loading type	Boundary Condition	a/h	a/b 0.25	0.50	0.75	1.00
Uniaxial compression	SSSS	10	202.39	185.66	158.49	126.46
		20	211.71	194.46	166.46	133.28
		50	214.75	197.34	169.06	135.50
		100	215.20	197.76	169.45	135.83
	CCCC	10	83.36	74.71	53.95	30.57
		20	206.02	197.99	178.92	149.34
		50	216.74	208.52	188.95	158.01
		100	218.48	210.25	190.59	159.44
Biaxial compression	SSSS	10	124.67	122.34	129.55	126.45
		20	131.30	128.73	136.11	133.28
		50	134.76	130.92	138.34	135.50
		100	139.61	131.40	138.70	135.83
	CCCC	10	95.20	89.42	84.97	88.84
		20	110.04	101.61	100.35	98.42
		50	127.18	108.22	106.21	103.46
		100	137.68	111.35	107.66	104.51

Table 9. Percentage increase ($\mathcal{I}_b$) in normalised critical buckling strength of HFRP-2.

Loading type	Boundary condition	a/h	a/b 0.25	0.50	0.75	1.00
Uniaxial compression	SSSS	10	128.71	119.59	107.37	96.05
		20	140.90	131.06	117.43	104.13
		50	145.00	134.93	120.85	106.92
		100	145.62	135.51	121.37	107.34
	CCCC	10	80.58	72.06	51.62	28.60
		20	131.02	127.49	121.00	112.66
		50	145.06	141.11	133.45	123.11
		100	147.44	143.42	135.57	124.91
Biaxial compression	SSSS	10	102.46	96.04	107.36	96.05
		20	110.80	104.12	117.43	104.13
		50	113.93	106.91	120.85	106.92
		100	115.21	107.33	121.37	107.34
	CCCC	10	85.98	86.22	86.77	91.10
		20	102.21	100.98	99.72	109.20
		50	112.79	109.36	107.28	118.95
		100	118.51	110.85	108.62	120.66

Based on the parametric study following salient features of a hybrid laminate are observed:

1. Normalised critical buckling strength for all types of laminates with a constant span to thickness ratio (a/h) increases with increase in aspect ratio (a/b).
2. Normalised critical buckling strength for all types of laminates of constant aspect ratio (a/b) also increases with increase in span to thickness ratio (a/h).
3. Normalised critical buckling strengths for both HFRP laminates are found significantly higher than corresponding GFRP laminates.

4. Hybridisation scheme plays an important role while designing, such as, under uniaxial loading condition HFRP-1 demonstrates better performance over HFRP-2.

5.2. Dynamic analysis

Similar to stability analysis, the effect of the percentage of hybridisation is studied during the dynamic analysis, specifically focusing on the natural frequencies of laminates. In addition to the effect of hybridisation on fundamental frequency, two other frequencies are also studied for the laminate geometries and boundary conditions.

5.2.1. Effect of hybridisation on modal behaviour in hybrid laminate

In the case of free vibration analysis, the percent of hybridisation of square-shaped laminate is varied from 0% to 50%. Significant improvement of natural frequencies is observed in both HFRP laminates compared to the pure GFRP laminate (Figure 8). From Figure 8, it can be seen that irrespective of thickness ratio, with increase in percentage of hybridisation a clear sign of increase in modal frequency is observed in both the HFRP laminates.

To quantify the competitive performance between HFRP-1 and HFRP-2, the percentage improvement of natural frequency ($\mathcal{I}_f$) in HFRP laminates are compared to original GFRP laminate and is calculated using the following equation

$$\mathcal{I}_f(\%) = \frac{\omega^{HFRP} - \omega^{GFRP}}{\omega^{GFRP}} \times 100 \tag{36}$$

The results of increase in natural frequencies for HFRP-1 and HFRP-2 laminates are shown in Figures 9 and 10, respectively. It is evident that the increase in the percentage of hybridisation in HFRP laminates would increase in natural frequency compared to GFRP laminate. Based on the results, it is clear that for HFRP-1 laminates the fundamental frequency can be increased over 50% (for all a/h ratio). On the other hand, for HFRP-2 laminates increase in fundamental frequency does not exceed 50%. In HFRP-1 laminates the rate of increase does not show a steady trend for all three modal frequencies. This trend could be attributed to the alignment of carbon fibres only along the longitudinal direction of HFRP-1 laminate, resulting in the transverse direction weaker

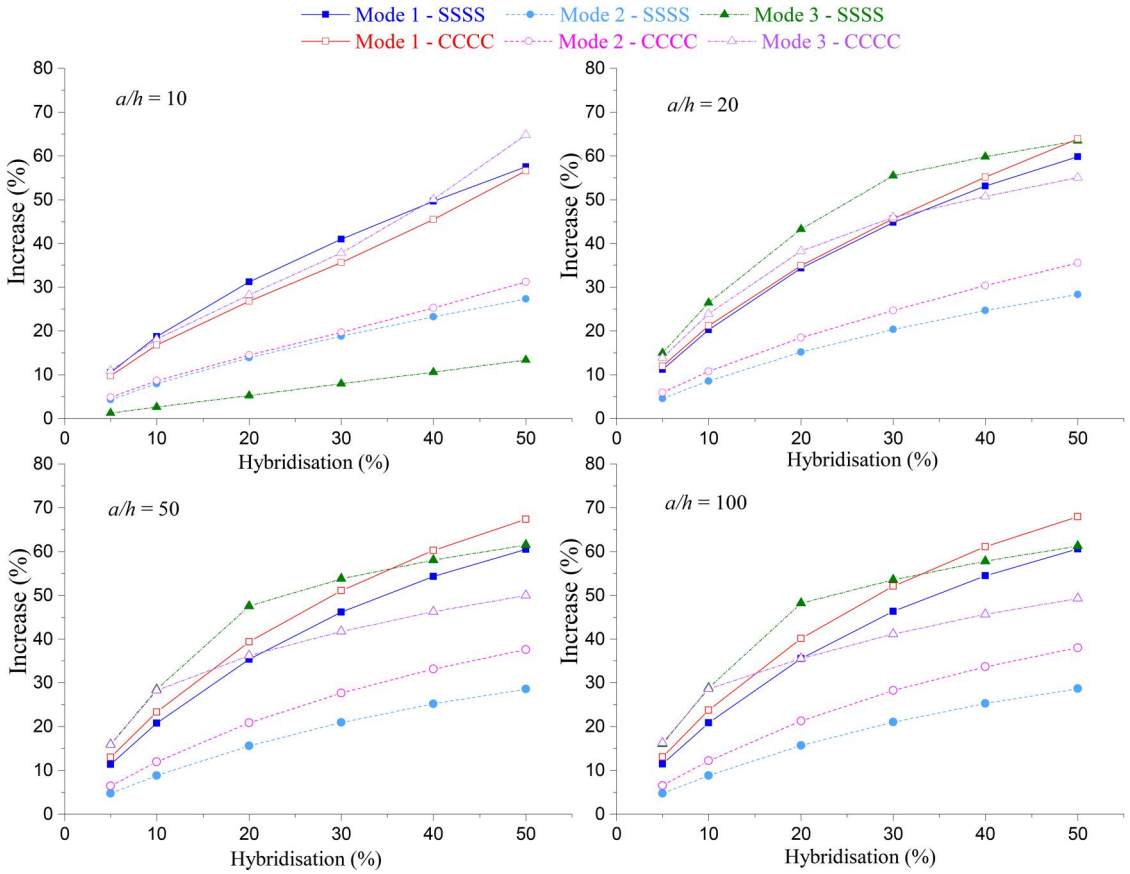

Figure 9. Increase of natural frequencies of HFRP-1 laminate tor GFRP laminate.

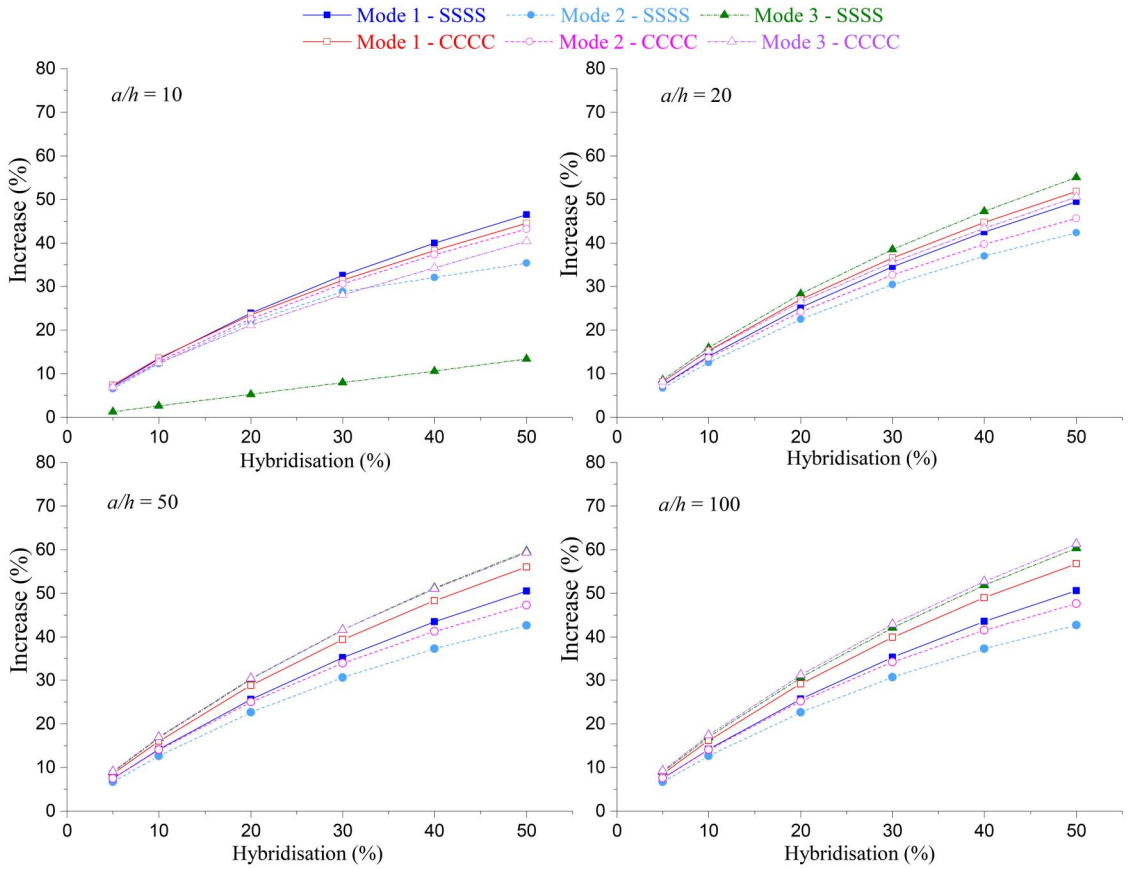

Figure 10. Increase of natural frequencies of HFRP-2 laminate tor GFRP laminate.

in stiffness and formation of low magnitude second and third modal frequencies. Contrary to the HFRP-1 laminate, it is noted that the rate of increase is very consistent for HFRP-2 laminates. This is due to uniform distribution of carbon fibre across both longitudinal and transverse directions.

5.2.2. Effect of aspect ratio on natural frequencies of hybrid laminates

Finally, the effect of laminate aspect ratio is studied considering 50% fibre hybridisation. Similar to the previous analysis the specimens are studied for both the boundary conditions keeping the percentage of hybridisation 50% and the assumption of equal laminate thickness. A comparison between the natural frequencies of the HFRP laminates and pure GFRP laminate is performed and given in Tables 10 and 11. It is to be noted that the $\mathcal{I}_f$ in HFRP laminates decreases with the increase of aspect ratio. The only exception is identified for thick plate with lowest aspect ratio (0.25) for simply support boundary condition. This could be due to formation of new modes at lower frequencies. At this geometric configuration the laminate will behave more of 3D beam than a plate. On the other hand, the $\mathcal{I}_f$ increases with increase in the span-to-thickness ratio (a/h). This indicates that for thinner plates the fundamental frequency can be improved significantly. Additionally, it is observed

Table 10. Percentage increase ($\mathcal{I}_f$) in natural frequency of HFRP-1 laminate over pure GFRP laminate.

Boundary condition	a/h	a/b			
		0.25	0.50	0.75	1.00
SSSS	10	13.37	76.83	68.24	57.50
	20	82.62	79.49	70.75	59.77
	50	85.55	80.34	71.56	60.50
	100	85.68	80.47	71.68	60.61
CCCC	10	74.78	72.43	66.37	56.54
	20	82.33	79.93	73.93	63.89
	50	85.99	83.57	77.53	67.34
	100	86.61	84.18	78.14	67.92

Table 11. Percentage increase ($\mathcal{I}_f$) in natural frequency of HFRP-2 laminate over pure GFRP laminate.

Boundary condition	a/h	a/b			
		0.25	0.50	0.75	1.00
SSSS	10	13.37	55.02	50.66	46.50
	20	62.33	58.99	54.23	49.44
	50	63.70	60.30	55.43	50.44
	100	63.91	60.50	55.61	50.59
CCCC	10	47.59	46.76	45.59	44.57
	20	58.04	56.87	54.68	51.84
	50	63.50	62.20	59.60	55.97
	100	64.46	63.13	60.48	56.72

that the magnitude of increase in natural frequency is higher in HFRP-1 laminates than HFRP-2 laminates. This indicates placing carbon fibre layups at the outer most surface which results in better dynamic performance in the HFRP-1 laminates.

6. Conclusion

This article highlights the advantage of fibre hybridisation in laminated composites as a cost-effective, smart, and sustainable design solution to practical structural applications. Application of hybrid laminates is still underrated in the industrial setting. However, in many industry sectors, hybrid laminates have the potential to improve structural performance over lower strength composite laminates; in particular to a sustainable implementation of bio-fibre based composites in structural application. Bio-fibre based composites are not yet well accepted in many industries due to their poor strength and quicker rate of environmental degradation. Often three-dimensional models are required to appropriately capture the structural response of hybrid laminates due to fibre hybridisation. One of the major challenges in the use of hybrid laminate lies in the computation cost involved while performing numerical analysis. Static analysis of composite laminates using zigzag effect is a popular approach over three-dimensional analysis of laminates. However, the zigzag theory is not much explored for stability and dynamic analysis due to additional complexity to compute geometric stiffness and mass matrices. In this article, the existing zigzag formulation [52] is further extended to perform stability and dynamic analysis. A methodology is presented to formulate and implement the mass and geometric stiffness matrices for computation considering the zigzag effect. Finally, the formulation is numerically implemented in a two-dimensional framework to solve stability and free-vibration problems. A C^0 continuous RHZT-based formulation ensured the continuity of transverse shear stresses at the layer interfaces. The proposed formulation is numerically implemented in the finite element framework using an eight-noded isoparametric quadratic plate bending element. First, the formulation is numerically verified for its accuracy with respect to published results. Two cross-ply laminates are used in the verification study. Mesh objectivity in the numerical solution is verified using five discretisations. Based on this study, compared to RFZT formulation, the proposed RHZT formulation provides more accurate numerical results in predicting buckling strengths and natural frequencies. Additionally, the higher efficiency of the framework for different boundary conditions have been verified. Next, an extensive parametric study is performed by considering parameters such as aspect ratio, span-to-thickness ratio, boundary conditions and percentage of hybridisation. For this purpose two different HFRP laminate configurations with same percentage of hybridisation are compared. Significant increase in critical buckling strengths and natural frequencies is observed in the both hybrid laminates compared to pure GFRP laminates. The parametric study involving the percentage of hybridisation clearly demonstrates enhancement in the structural performance of hybrid laminates. The comparison between the performance of two HFRP laminates enables the capability of tailoring laminates for intended application which will lead to sustainable and cost-effective design. Therefore, prior numerical analysis is strongly recommended before manufacturing laminates, specially the sequence of CFRP layups in a HFRP laminate.

Based on the analysis results, the following needs are identified for future work.

1. The parametric study identified that the performance of a hybrid laminate can be further tailored. Based on the application requirement, necessary optimisation techniques need to be employed.
2. In this study the material is assumed to be linear elastic. However, in reality materials demonstrate nonlinear and inelastic behaviour under service conditions. Therefore, an appropriate constitutive model can be incorporated to capture the nonlinear and inelastic effect within the material.
3. The proposed framework is developed in a deterministic setting. Defects in laminates due to material variability, manufacturing imperfection has significant effects on the performance of composite laminates. Therefore, stochastic aspects of the analysis remain an open area of future research [54, 55].
4. Finally, to reliably employ the proposed model in practice the model parameters can be calibrated and validated with experimental data. Uncertainty quantification of this computational model needs to be further performed.

Disclosure statement

No potential conflict of interest was reported by the authors.

References

[1] A. E. H. Love, "The small free vibrations and deformation of a thin elastic shell," *Philosoph. Trans. Roy. Soc. London*, vol. 179, pp. 491–546, 1888.

[2] S. Srinivas and A. K. Rao, "Bending, vibration and buckling of simply supported thick orthotropic rectangular plates and laminates," *Int. J. Solids Struct.*, vol. 6, no. 11, pp. 1463–1481, 1970. DOI: 10.1016/0020-7683(70)90076-4.

[3] A. K. Noor, "Stability of multilayered composite plates," *Fibre Sci. Technol.*, vol. 8, no. 2, pp. 81–89, 1975. DOI: 10.1016/0015-0568(75)90005-6.

[4] R. Bhattacharyya, S. Mahadevan and P. K. Basu, "Computationally efficient multiscale modeling for probabilistic analysis of CFRP composites with micro-scale spatial randomness," *Compos. Struct.*, vol. 280, pp. 114884, 2021. DOI: 10.1016/j.compstruct.2021.114884.

[5] P. C. Yang, C. H. Norris and Y. Stavsky, "Elastic wave propagation in heterogeneous plates," *Int. J. Solids Struct.*, vol. 2, no. 4, pp. 665–684, 1966. DOI: 10.1016/0020-7683(66)90045-X.

[6] J. M. Whitney and N. J. Pagano, "Shear deformation in heterogeneous anisotropic plates," *J. Appl. Mechanics*, vol. 37, no. 4, pp. 1031–1036, 1970. 12 DOI: 10.1115/1.3408654.

[7] B. O. Baba, "Buckling behavior of laminated composite plates," *J. Reinforce Plastic Compos.*, vol. 26, no. 16, pp. 1637–1655, 2007. DOI: 10.1177/0731684407079515.

[8] H. Nguyen-Van, N. Mai-Duy, W. Karunasena and T. Tran-Cong, "Buckling and vibration analysis of laminated composite plate/shell structures via a smoothed quadrilateral flat shell element with in-plane rotations," *Comput. Struct.*, vol. 89, no. 7-8, pp. 612–625, 2011. DOI: 10.1016/j.compstruc.2011.01.005.

[9] A. J. M. Ferreira, L. M. Castro, C. M. C. Roque, J. N. Reddy and S. Bertoluzza, "Buckling analysis of laminated plates by wavelets," *Comput. Struct.*, vol. 89, no. 7-8, pp. 626–630, 2011. DOI: 10.1016/j.compstruc.2011.01.007.

[10] Y. Narita and A. W. Leissa, "Buckling studies for simply supported symmetrically laminated rectangular plates," *Int. J. Mech. Sci.*, vol. 32, no. 11, pp. 909–924, 1990. DOI: 10.1016/0020-7403(90)90063-O.

[11] B. Baharlou and A. W. Leissa, "Vibration and buckling of generally laminated composite plates with arbitrary edge conditions," *Int. J. Mech. Sci.*, vol. 29, no. 8, pp. 545–555, 1987. DOI: 10.1016/0020-7403(87)90026-9.

[12] K. M. Liew, "Solving the vibration of thick symmetric laminates by Reissner/Mindlin plate theory and Thep-Ritz method," *J. Sound Vib.*, vol. 198, no. 3, pp. 343–360, 1996. DOI: 10.1006/jsvi.1996.0574.

[13] J. N. Reddy, "A simple higher-order theory for laminated composite plates," *J. Appl. Mech.*, vol. 51, no. 4, pp. 745–752, 1984. 12 DOI: 10.1115/1.3167719.

[14] T. Kant, "Numerical analysis of thick plates," *Comput. Method Appl. Mech. Eng.*, vol. 31, no. 1, pp. 1–18, 1982. DOI: 10.1016/0045-7825(82)90043-3.

[15] N. D. Phan and J. N. Reddy, "Analysis of laminated composite plates using a higher-order shear deformation theory," *Numer. Meth Eng.*, vol. 21, no. 12, pp. 2201–2219, 1985. DOI: 10.1002/nme.1620211207.

[16] J. N. Reddy and N. D. Phan, "Stability and vibration of isotropic, orthotropic and laminated plates according to a higher-order shear deformation theory," *J. Sound Vib.*, vol. 98, no. 2, pp. 157–170, 1985. DOI: 10.1016/0022-460X(85)90383-9.

[17] A. A. Khdeir and L. Librescu, "Analysis of symmetric cross-ply laminated elastic plates using a higher-order theory: Part II-buckling and free vibration," *Compos. Struct.*, vol. 9, no. 4, pp. 259–277, 1988. DOI: 10.1016/0263-8223(88)90048-7.

[18] M. E. Fares and A. M. Zenkour, "Buckling and free vibration of non-homogeneous composite cross-ply laminated plates with various plate theories," *Compos. Struct.*, vol. 44, no. 4, pp. 279–287, 1999. DOI: 10.1016/S0263-8223(98)00135-4.

[19] H.-T. Hu and W.-L. Tzeng, "Buckling analysis of skew laminate plates subjected to uniaxial in plane loads," *Thin-Walled Struct.*, vol. 38, no. 1, pp. 53–77, 2000. DOI: 10.1016/S0263-8231(00)00029-X.

[20] A. Chakrabarti and A. H. Sheikh, "Buckling of laminated composite plates by a new element based on higher order shear deformation theory," *Mech. Adv. Mater. Struct.*, vol. 10, no. 4, pp. 303–317, 2003. DOI: 10.1080/10759410306754.

[21] H.-T. Hu, C.-H. Yang and F.-M. Lin, "Buckling analyses of composite laminate skew plates with material nonlinearity," *Compos. Part B: Eng.*, vol. 37, no. 1, pp. 26–36, 2006. DOI: 10.1016/j.compositesb.2005.05.004.

[22] A. Remil, K. H. Benrahou, K. Draiche, A. A. Bousahla and A. Tounsi, "A simple HSDT for bending, buckling and dynamic behavior of laminated composite plates," *Struct. Eng. Mech.*, vol. 70, no. 3, pp. 325–337, 2019.

[23] N. Grover, D. K. Maiti and B. N. Singh, "A new inverse hyperbolic shear deformation theory for static and buckling analysis of laminated composite and sandwich plates," *Compos. Struct.*, vol. 95, pp. 667–675, 2013. DOI: 10.1016/j.compstruct.2012.08.012.

[24] D. B. Singh and B. N. Singh, "New higher order shear deformation theories for free vibration and buckling analysis of laminated and braided composite plates," *Int. J. Mech. Sci.*, vol. 131-132, pp. 265–277, 2017. DOI: 10.1016/j.ijmecsci.2017.06.053.

[25] A. Chaubey, A. Kumar, A. Kwiatkowski, B. Barnat-Hunek, D. Widomski, and K. Marcin. Bi-axial buckling of laminated composite plates including cutout and additional mass. *Materials*, vol. 12, no. 11, pp. 1750, 2019. DOI: 10.3390/ma12111750.

[26] A. Attia, A. T. Berrabah, A. A. Bousahla, F. Bourada, A. Tounsi and S. R. Mahmoud, "Free vibration analysis of FG plates under thermal environment via a simple 4-unknown HSDT," *Steel Compos. Struct.*, vol. 41, no. 6, pp. 899–910, 2021.

[27] S. Srinivas, "A refined analysis of composite laminates," *J. Sound Vib.*, vol. 30, no. 4, pp. 495–507, 1973. DOI: 10.1016/S0022-460X(73)80170-1.

[28] A. Toledano and H. Murakami, "A composite plate theory for arbitrary laminate configurations," *J. Appl.*

Mech., vol. 54, no. 1, pp. 181–189, 1987. 03 DOI: 10.1115/1.3172955.

[29] D. H. Robbins, Jr. and J. N. Reddy, "Modelling of thick composites using a layerwise laminate theory," *Numer. Meth Eng.*, vol. 36, no. 4, pp. 655–677, 1993. DOI: 10.1002/nme.1620360407.

[30] K. N. Cho, C. W. Bert and A. G. Striz, "Free vibrations of laminated rectangular plates analyzed by higher order individual-layer theory," *J. Sound Vibration*, vol. 145, no. 3, pp. 429–442, 1991. DOI: 10.1016/0022-460X(91)90112-W.

[31] X. Li and D. Liu, "Zigzag theory for composite laminates," *AIAA J.*, vol. 33, no. 6, pp. 1163–1165, 1995. DOI: 10.2514/3.12671.

[32] M. D. Sciuva, "A refined transverse shear deformation theory for multilayered anisotropic plates," *In Atti Academia Sci di Torino*, vol. 118, pp. 279–295, 1984.

[33] M. Di Sciuva, "Multilayered anisotropic plate models with continuous interlaminar stresses," *Compos. Struct.*, vol. 22, no. 3, pp. 149–167, 1992. DOI: 10.1016/0263-8223(92)90003-U.

[34] D. Liu and X. Li, "An overall view of laminate theories based on displacement hypothesis," *J. Compos. Mater.*, vol. 30, no. 14, pp. 1539–1561, 1996. DOI: 10.1177/002199839603001402.

[35] H. Murakami, "Laminated Composite Plate Theory With Improved In-Plane Responses," *J. Appl. Mech.*, vol. 53, no. 3, pp. 661–666, 1986. DOI: 10.1115/1.3171828.

[36] A. Tessler, M. Di Sciuva and M. Gherlone, *Refinement of Timoshenko Beam Theory for Composite and Sandwich Beams Using Zigzag Kinematics*. Technical Report NASA/TP-2007-215086, NASA, 2007.

[37] A. Tessler, M. Di Sciuva and M. Gherlone, "A refined zigzag beam theory for composite and sandwich beams," *J. Compos. Mater.*, vol. 43, no. 9, pp. 1051–1081, 2009. DOI: 10.1177/0021998308097730.

[38] A. Tessler, M. Di Sciuva and M. Gherlone, *Refined Zigzag Theory for Homogeneous, Laminated Composite, and Sandwich Plates: A Homogeneous Limit Methodology for Zigzag Function Selection*. Technical Report NASA/TP-2010-216214, NASA, 2010.

[39] A. Tessler, M. Di Sciuva and M. Gherlone, "A consistent refinement of first-order shear deformation theory for laminated composite and sandwich plates using improved zigzag kinematics," *JOMMS*, vol. 5, no. 2, pp. 341–367, 2010. DOI: 10.2140/jomms.2010.5.341.

[40] T. Kant and P. B. Kulkarni, "A c° continuous linear beam/bilinear plate flexure element," *Comput. Struct.*, vol. 22, no. 3, pp. 413–425, 1986. DOI: 10.1016/0045-7949(86)90046-5.

[41] A. Chakrabarti and A. H. Sheikh, "Buckling of laminated sandwich plates subjected to partial edge compression," *Int. J. Mech. Sci.*, vol. 47, no. 3, pp. 418–436, 2005. DOI: 10.1016/j.ijmecsci.2005.01.005.

[42] P. Nali, E. Carrera and S. Lecca, "Assessments of refined theories for buckling analysis of laminated plates," *Compos. Struct.*, vol. 93, no. 2, pp. 456–464, 2011. DOI: 10.1016/j.compstruct.2010.08.035.

[43] S. K. Singh and A. Chakrabarti, "Buckling analysis of laminated composite plates using an efficient c0 FE model," *Lat. Am. J. Solid. Struct*, vol. 9, no. 3, pp. 1–13, 2012. DOI: 10.1590/S1679-78252012000300003.

[44] R. Vescovini and L. Dozio, "Exact refined buckling solutions for laminated plates under uniaxial and biaxial loads," *Compos. Struct.*, vol. 127, pp. 356–368, 2015. DOI: 10.1016/j.compstruct.2015.03.003.

[45] R. Sahoo and B. N. Singh, "Assessment of inverse hyperbolic zigzag theory for buckling analysis of laminated composite and sandwich plates using finite element method," *Arch Appl Mech*, vol. 91, no. 1, pp. 169–186, 2021. DOI: 10.1007/s00419-020-01761-9.

[46] S. Kapuria and J. K. Nath, "On the accuracy of recent global-local theories for bending and vibration of laminated plates," *Compos. Struct.*, vol. 95, pp. 163–172, 2013. DOI: 10.1016/j.compstruct.2012.06.018.

[47] A. Treviso, D. Mundo and M. Tournour, "Dynamic response of laminated structures using a refined zigzag theory shell element," *Composite Structures*, vol. 159, pp. 197–205, 2017. DOI: 10.1016/j.compstruct.2016.09.026.

[48] S. Sarangan and B. N. Singh, "Evaluation of free vibration and bending analysis of laminated composite and sandwich plates using non-polynomial zigzag models: c0 finite element formulation," *Aerosp Sci. Technol.*, vol. 68, pp. 496–508, 2017. DOI: 10.1016/j.ast.2017.06.001.

[49] H. Tanzadeh and H. Amoushahi, "Buckling and free vibration analysis of piezoelectric laminated composite plates using various plate deformation theories," *Eur. J. Mech. A/Solids*, vol. 74, pp. 242–256, 2019. DOI: 10.1016/j.euromechsol.2018.11.013.

[50] N. Belbachir, *et al.*, "A refined quasi-3d theory for stability and dynamic investigation of cross-ply laminated composite plates on Winkler-Pasternak foundation," *Struct. Eng. Mech.*, vol. 85, no. 4, pp. 433–443, 2023.

[51] S. Abdelbari, A. Attia, F. Bourada, A. A. Bousahla, A. Tounsi and M. H. Ghazwani, "Investigation of dynamic characteristics of imperfect FG beams on the Winkler-Pasternak foundation under thermal loading," *Phys Mesomech*, vol. 26, no. 5, pp. 557–572, 2023. DOI: 10.1134/S1029959923050089.

[52] D. Biswas and C. Ray, "An improved isoparametric quadratic element based on refined zigzag theory to compute interlaminar stresses of multilayered anisotropic plates," *Numer. Meth Eng.*, vol. 119, no. 12, pp. 1245–1278, 2019. DOI: 10.1002/nme.6090.

[53] L. Liu, L. P. Chua and D. N. Ghista, "Mesh-free radial basis function method for static, free vibration and buckling analysis of shear deformable composite laminates," *Compos. Struct.*, vol. 78, no. 1, pp. 58–69, 2007. DOI: 10.1016/j.compstruct.2005.08.010.

[54] R. Bhattacharyya and D. Adams, "Multiscale analysis of multi-directional composite laminates to predict stiffness and strength in the presence of micro-defects," *Compos. Part C: Open Access*, vol. 6, pp. 100189, 2021. DOI: 10.1016/j.jcomc.2021.100189.

[55] R. Bhattacharyya and S. Mahadevan, "Calibration and validation of multiscale model for ultimate strength prediction of composite laminates under uncertainty," *ASCE-ASME J Risk Uncert Engrg Sys Part B Mech Eng*, vol. 8, no. 2, pp. 021205, 2022.